



UNIVERSIDAD NACIONAL AUTÓNOMA DE MÉXICO

INSTITUTO DE ENERGÍAS RENOVABLES

VALIDATION OF TURBULENCE MODELS FOR
REPRESENTING PRESSURE COEFFICIENTS FOR
NATURAL VENTILATION PURPOSES ON AN
ISOLATED LOW-RISE BUILDING

S U P P L E M E N T A R Y
M A T E R I A L

AUTHORS:

MSE. ÁNGEL SÁNCHEZ CRUZ

DR. EDUARDO RAMOS MORA

DR. SAÚL PIEDRA GONZÁLEZ

DR. EDMUNDO AMAYA GALLARDO

DR. VLADIMIR ARTURO REYES HERRERA

Contents

Contents	3
List of Figures	5
List of Tables	9
1 Validation of Profiles Through Domain, Pressure Coefficient Contour Maps and Qualitative Assessment of Wall-Averaged Pressure Coefficient	11
1.1 Velocity and Turbulence Profiles Through Domain	13
1.2 Contour Maps of Pressure Coefficients Derived from CFD Simulations	19
1.3 Quantitative analysis of wall-averaged pressure coefficient $\overline{C_P}$	24
2 Local CFD Pressure Coefficient Comparison with BDA and TPU Databases	29
2.1 Pressure Coefficient Contour Maps. BDA vs CFD	31
2.2 Pressure Coefficient Contour Maps. TPU vs CFD	40
2.3 BDA and TPU Normalized Mean Square Error (<i>NMSE</i>) and Normalized Root Mean Square Error (ε)	52
2.4 Comparison Of Pressure Coefficients At Wall Center-lines With Respect To Databases	54
2.5 Turbulent Kinetic Energy and Turbulent Viscosity Fields in Parallel and Cross-Sectional Planes	59
2.6 Stream-lines	76

List of Figures

1.1	Velocity and turbulent profiles, STD $k-\epsilon$	13
1.2	Velocity and turbulent profiles, Realizable $k-\epsilon$	14
1.3	Velocity and turbulent profiles, RNG $k-\epsilon$	15
1.4	Velocity and turbulent profiles, STD $k-\omega$	16
1.5	Velocity and turbulent profiles, SST $k-\omega$	17
1.6	C_P contour maps, STD $k-\epsilon$	19
1.7	C_P contour maps, Realizable $k-\epsilon$	20
1.8	C_P contour maps, RNG $k-\epsilon$	21
1.9	C_P contour maps, STD $k-\omega$	22
1.10	C_P contour maps, SST $k-\omega$	23
2.1	Experimental BDA and TPU tap position	29
2.2	C_P contour maps, BDA 0°	31
2.3	C_P contour maps at BDA tap coordinates, STD $k-\epsilon$, 0°	31
2.4	C_P contour maps at BDA tap coordinates, Realizable $k-\epsilon$, 0°	32
2.5	C_P contour maps at BDA tap coordinates, RNG $k-\epsilon$, 0°	32
2.6	C_P contour maps at BDA tap coordinates, STD $k-\omega$, 0°	33
2.7	C_P contour maps at BDA tap coordinates, SST $k-\omega$, 0°	33
2.8	C_P contour maps, BDA 30°	34
2.9	C_P contour maps at BDA tap coordinates, STD $k-\epsilon$, 30°	34
2.10	C_P contour maps at BDA tap coordinates, Realizable $k-\epsilon$, 30°	35
2.11	C_P contour maps at BDA tap coordinates, RNG $k-\epsilon$, 30°	35
2.12	C_P contour maps at BDA tap coordinates, STD $k-\omega$, 30°	36
2.13	C_P contour maps at BDA tap coordinates, SST $k-\omega$, 30°	36
2.14	C_P contour maps, BDA 45°	37
2.15	C_P contour maps at BDA tap coordinates, STD $k-\epsilon$, 45°	37
2.16	C_P contour maps at BDA tap coordinates, Realizable $k-\epsilon$, 45°	38
2.17	C_P contour maps at BDA tap coordinates, RNG $k-\epsilon$, 45°	38
2.18	C_P contour maps at BDA tap coordinates, STD $k-\omega$, 45°	39

2.19	C_P contour maps at BDA tap coordinates, SST $k-\omega$, 45°	39
2.20	C_P contour maps, TPU 0°	40
2.21	C_P contour maps at TPU tap coordinates, STD $k-\epsilon$, 0°	40
2.22	C_P contour maps at TPU tap coordinates, Realizable $k-\epsilon$, 0°	41
2.23	C_P contour maps at TPU tap coordinates, RNG $k-\epsilon$, 0°	41
2.24	C_P contour maps at TPU tap coordinates, STD $k-\omega$, 0°	42
2.25	C_P contour maps at TPU tap coordinates, SST $k-\omega$, 0°	42
2.26	C_P contour maps, TPU 15°	43
2.27	C_P contour maps at TPU tap coordinates, STD $k-\epsilon$, 15°	43
2.28	C_P contour maps at TPU tap coordinates, Realizable $k-\epsilon$, 15°	44
2.29	C_P contour maps at TPU tap coordinates, RNG $k-\epsilon$, 15°	44
2.30	C_P contour maps at TPU tap coordinates, STD $k-\omega$, 15°	45
2.31	C_P contour maps at TPU tap coordinates, SST $k-\omega$, 15°	45
2.32	C_P contour maps, TPU 30°	46
2.33	C_P contour maps at TPU tap coordinates, STD $k-\epsilon$, 30°	46
2.34	C_P contour maps at TPU tap coordinates, Realizable $k-\epsilon$, 30°	47
2.35	C_P contour maps at TPU tap coordinates, RNG $k-\epsilon$, 30°	47
2.36	C_P contour maps at TPU tap coordinates, STD $k-\omega$, 30°	48
2.37	C_P contour maps at TPU tap coordinates, SST $k-\omega$, 30°	48
2.38	C_P contour maps, TPU 45°	49
2.39	C_P contour maps at TPU tap coordinates, STD $k-\epsilon$, 45°	49
2.40	C_P contour maps at TPU tap coordinates, Realizable $k-\epsilon$, 45°	50
2.41	C_P contour maps at TPU tap coordinates, RNG $k-\epsilon$, 45°	50
2.42	C_P contour maps at TPU tap coordinates, STD $k-\omega$, 45°	51
2.43	C_P contour maps at TPU tap coordinates, SST $k-\omega$, 45°	51
2.44	NMSE refered to BDA basedata per wall for all turbulence models.	52
2.45	NMSE refered to TPU basedata per wall for all turbulence models.	53
2.46	ε refered to BDA basedata per wall for all turbulence models.	53
2.47	ε refered to TPU basedata per wall for all turbulence models.	53
2.48	Center-lines at BDA and TPU tap position	54
2.49	BDA C_P at horizontal center-line	55
2.50	BDA C_P at vertical center-line	56

2.51 TPU C_P at horizontal center-line	57
2.52 TPU C_P at vertical center-line	58
2.53 Turbulent kinetic energy (k) field in the parallel flow plane for turbulence models at 0°	59
2.54 Turbulent viscosity (ν_t) field in the parallel flow plane for turbulence models at 0°	60
2.55 Cross-sectional turbulent kinetic energy (k) field for turbulence models at 0°	61
2.56 Cross-sectional turbulent viscosity (ν_t) field for turbulence models at 0°	62
2.57 Turbulent kinetic energy (k) field in the parallel flow plane for turbulence models at 15°	63
2.58 Turbulent viscosity (ν_t) field in the parallel flow plane for turbulence models at 15°	64
2.59 Cross-sectional turbulent kinetic energy (k) field for turbulence models at 15°	65
2.60 Cross-sectional turbulent viscosity (ν_t) field for turbulence models at 15°	66
2.61 Turbulent kinetic energy (k) field in the parallel flow plane for turbulence models at 30°	67
2.62 Turbulent viscosity (ν_t) field in the parallel flow plane for turbulence models at 30°	68
2.63 Cross-sectional turbulent kinetic energy (k) field for turbulence models at 30°	69
2.64 Cross-sectional turbulent viscosity (ν_t) field for turbulence models at 30°	70
2.65 Turbulent kinetic energy (k) field in the parallel flow plane for turbulence models at 45°	71
2.66 Turbulent viscosity (ν_t) field in the parallel flow plane for turbulence models at 45°	72
2.67 Cross-sectional turbulent kinetic energy (k) field for turbulence models at 45°	73

2.68	Cross-sectional turbulent viscosity (ν_t) field for turbulence models at 45°	74
2.69	U stream-lines, STD $k-\epsilon$	76
2.70	U stream-lines, Realizable $k-\epsilon$	77
2.71	U stream-lines, RNG $k-\epsilon$	78
2.72	U stream-lines, STD $k-\omega$	79
2.73	U stream-lines, SST $k-\omega$	80

List of Tables

1.1	Comparison of $\overline{C_P}$ on the walls. Databases, $k\text{-}\epsilon$ and $k\text{-}\omega$ turbulence models	25
1.2	Wall $\overline{C_P}$ relative error with respect to AIVC database	26
1.3	Wall $\overline{C_P}$ relative error with respect to BDA database	27
1.4	Wall $\overline{C_P}$ relative error with respect to TPU database	28

Chapter 1

Validation of Profiles Through Domain, Pressure Coefficient Contour Maps and Qualitative Assessment of Wall-Averaged Pressure Coefficient

Section 1.1 presents the validation of the velocity and turbulence profiles within the computational domain without building. These profiles were sampled at five distinct points, spanning from the inlet to the outlet of the *empty* domain. The theoretical velocity profile, u , is plotted to demonstrate that it traverses the domain without perturbations, ensuring that the turbulence profiles, I , k , ϵ , and ω , remain consistent throughout.

Section 1.2 presents the contour maps of pressure coefficients on the building faces for atmospheric boundary layer profile incidence angles of 0° , 15° , 30° , and 45° , derived from CFD simulations. The contour maps include results obtained using the STD $k-\epsilon$, Realizable $k-\epsilon$, RNG $k-\epsilon$, STD $k-\omega$, and SST $k-\omega$ turbulence models.

Section 1.3 presents a qualitative analysis of the wall-averaged pressure coefficient ($\overline{C_P}$), comparing the CFD results from this study with experimental data.

1.1 Velocity and Turbulence Profiles Through Domain

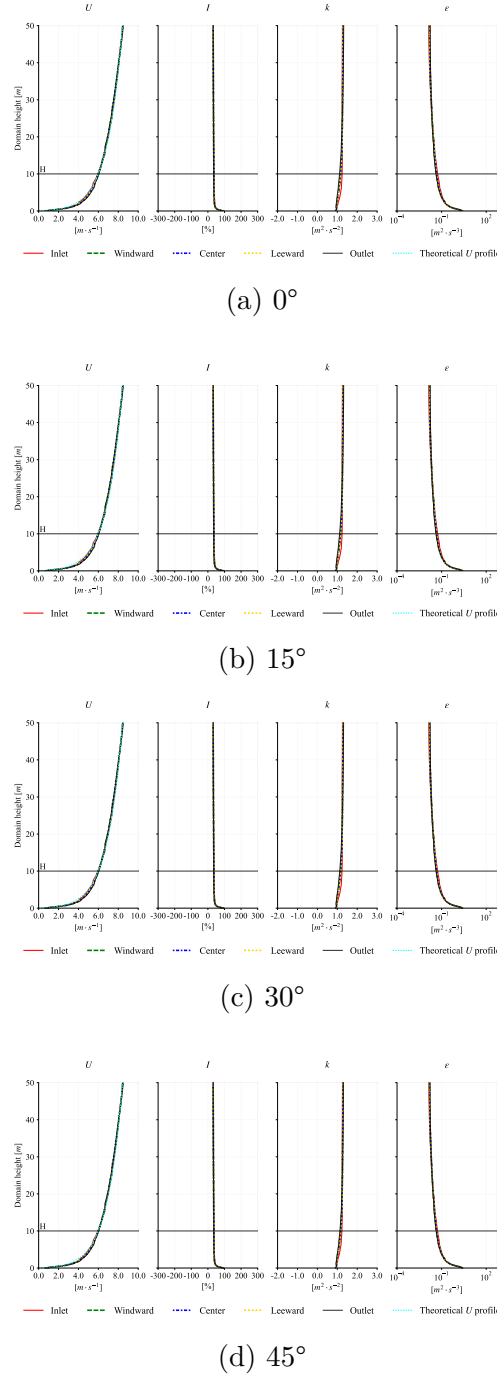
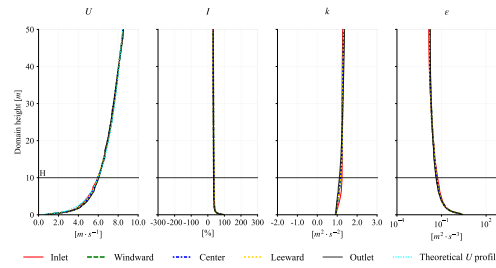
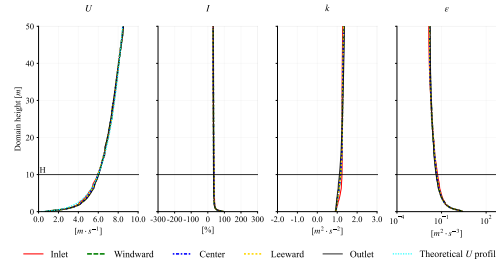


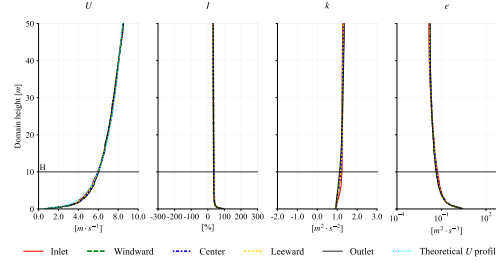
Figure 1.1: Velocity and turbulent profiles, STD k - ϵ



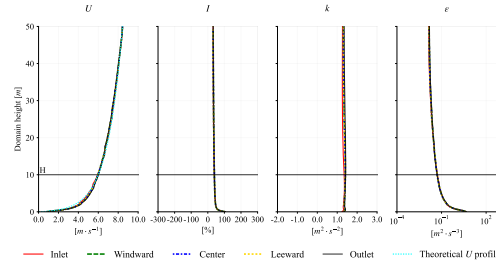
(a) 0°



(b) 15°

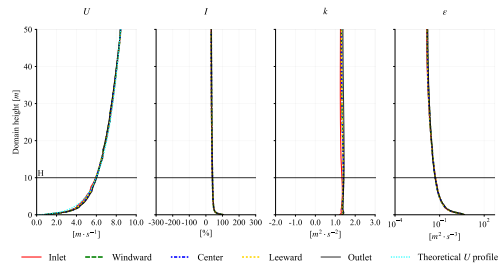


(c) 30°

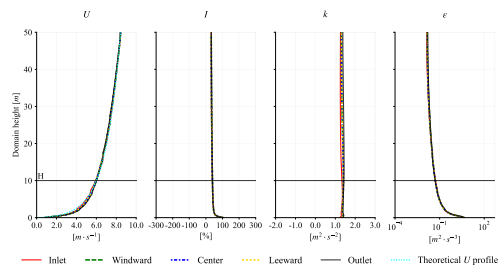


(d) 45°

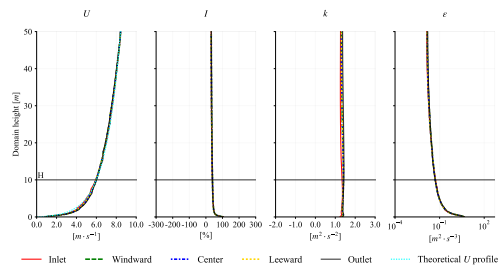
Figure 1.2: Velocity and turbulent profiles, Realizable k - ϵ



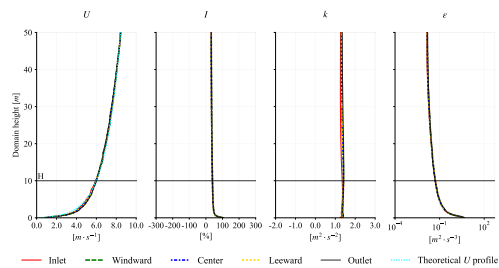
(a) 0°



(b) 15°

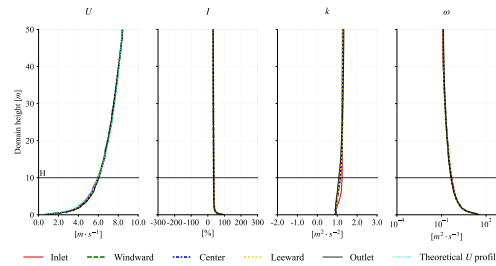


(c) 30°

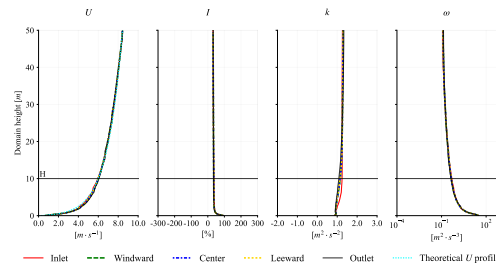


(d) 45°

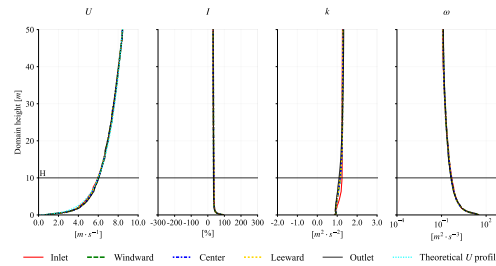
Figure 1.3: Velocity and turbulent profiles, RNG $k-\epsilon$



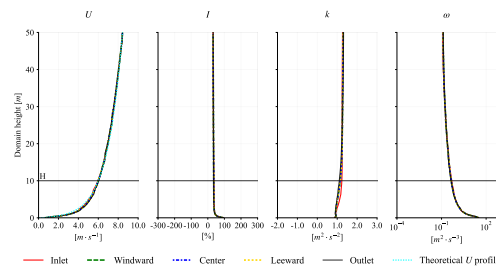
(a) 0°



(b) 15°

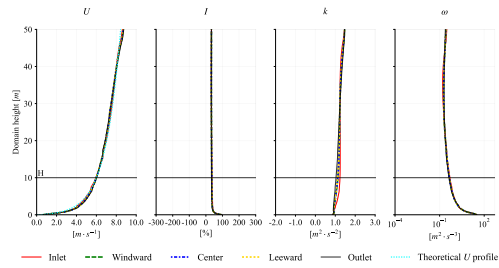


(c) 30°

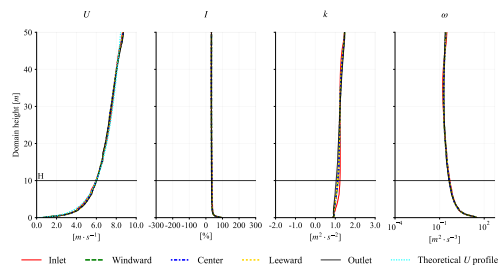


(d) 45°

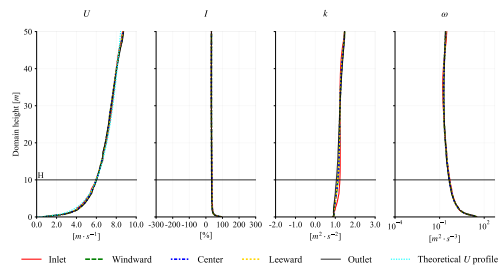
Figure 1.4: Velocity and turbulent profiles, STD $k-\omega$



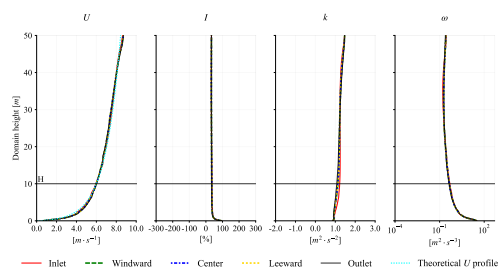
(a) 0°



(b) 15°



(c) 30°



(d) 45°

Figure 1.5: Velocity and turbulent profiles, SST $k-\omega$

1.2 Contour Maps of Pressure Coefficients Derived from CFD Simulations

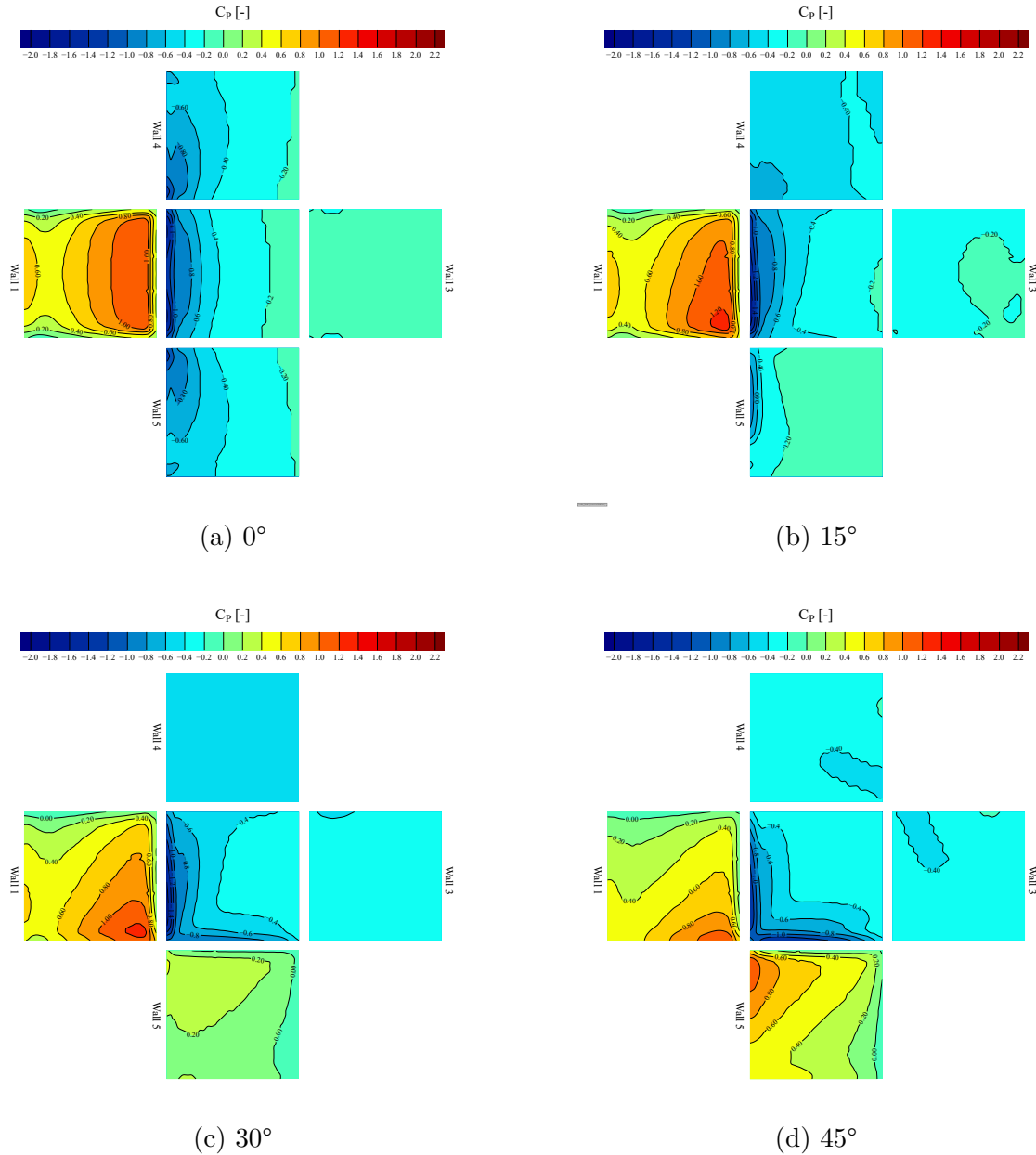


Figure 1.6: C_P contour maps, $STD\ k-\epsilon$

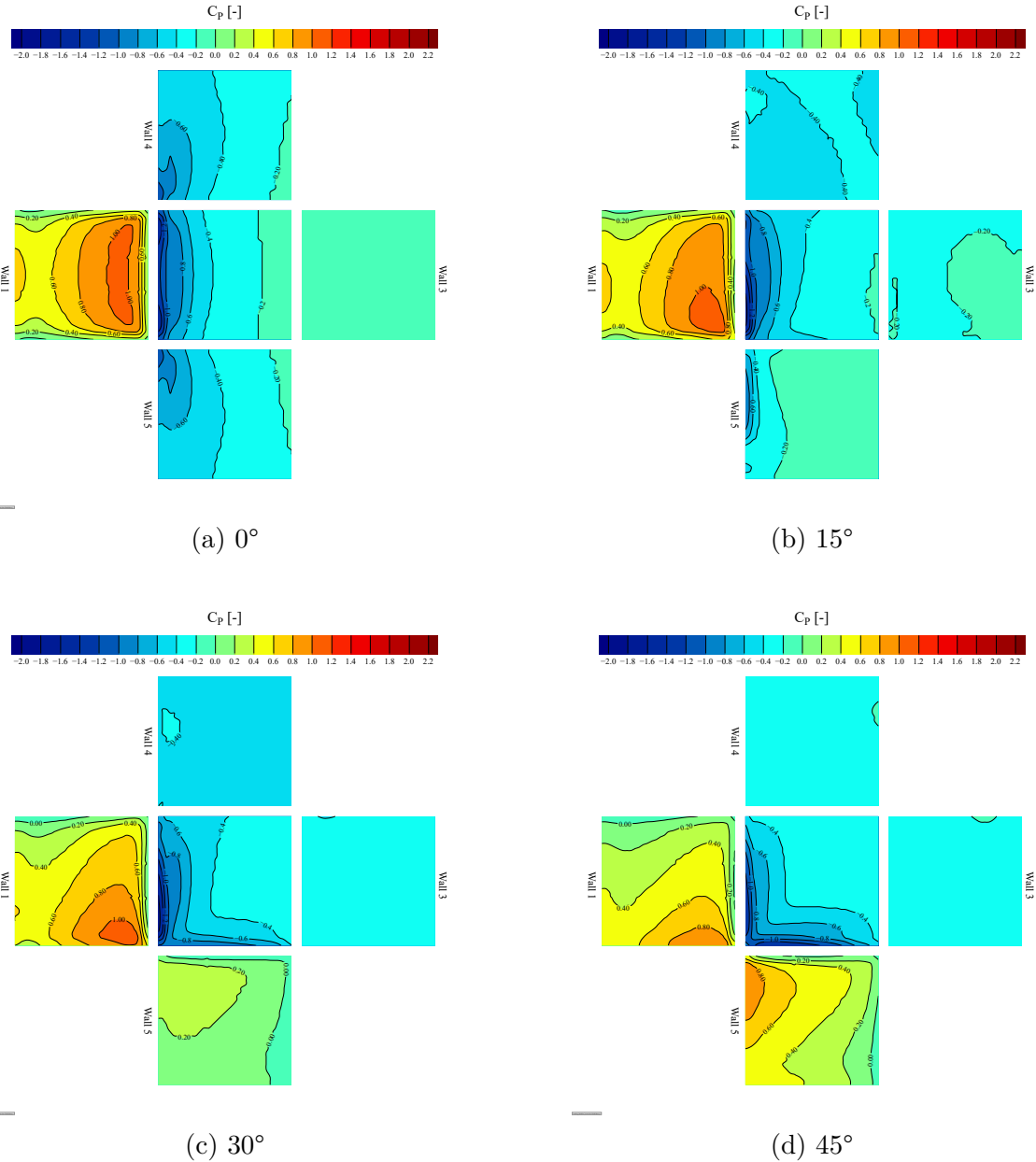


Figure 1.7: C_P contour maps, Realizable $k-\epsilon$

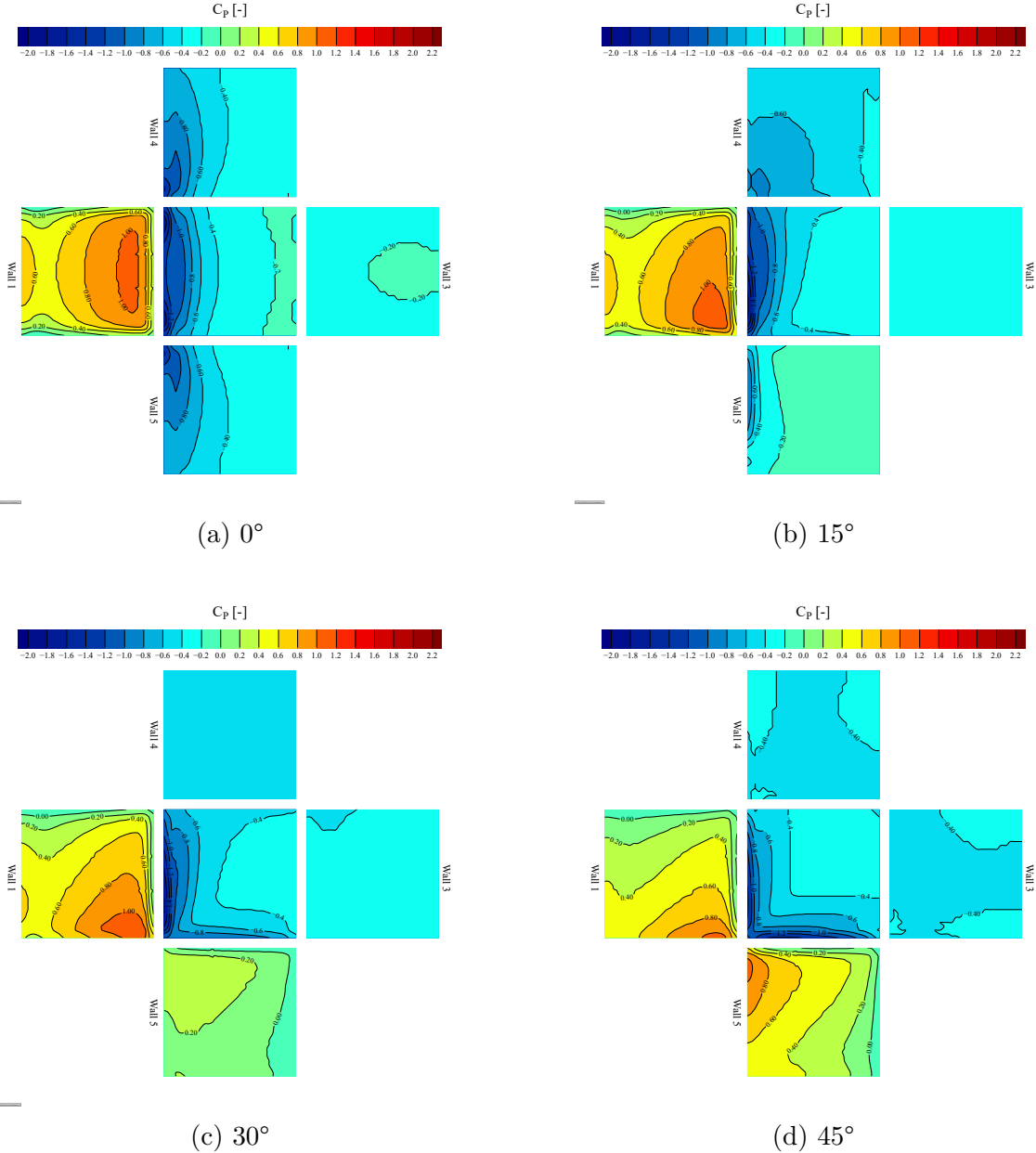


Figure 1.8: C_P contour maps, RNG $k-\epsilon$

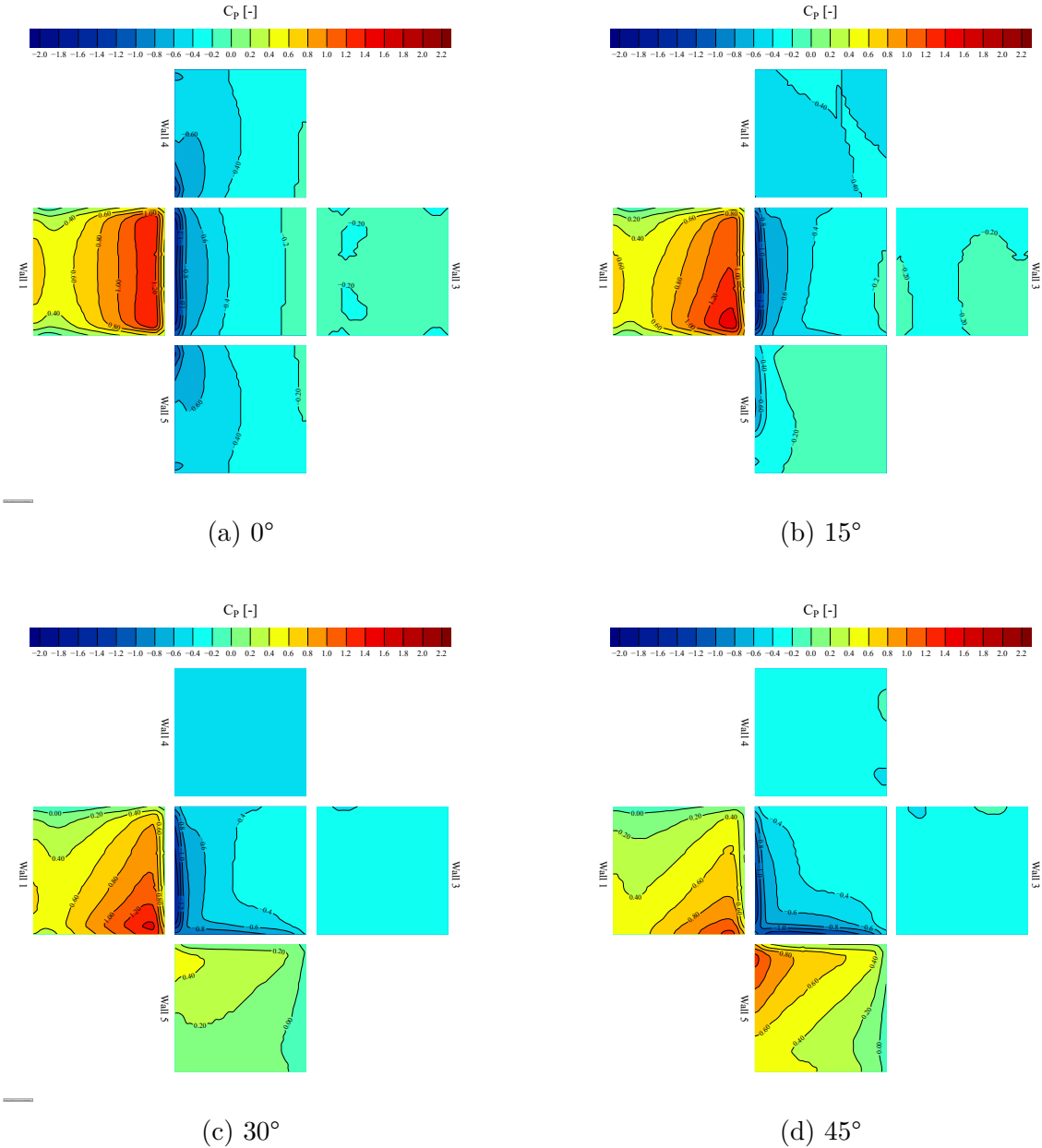


Figure 1.9: C_P contour maps, STD $k-\omega$

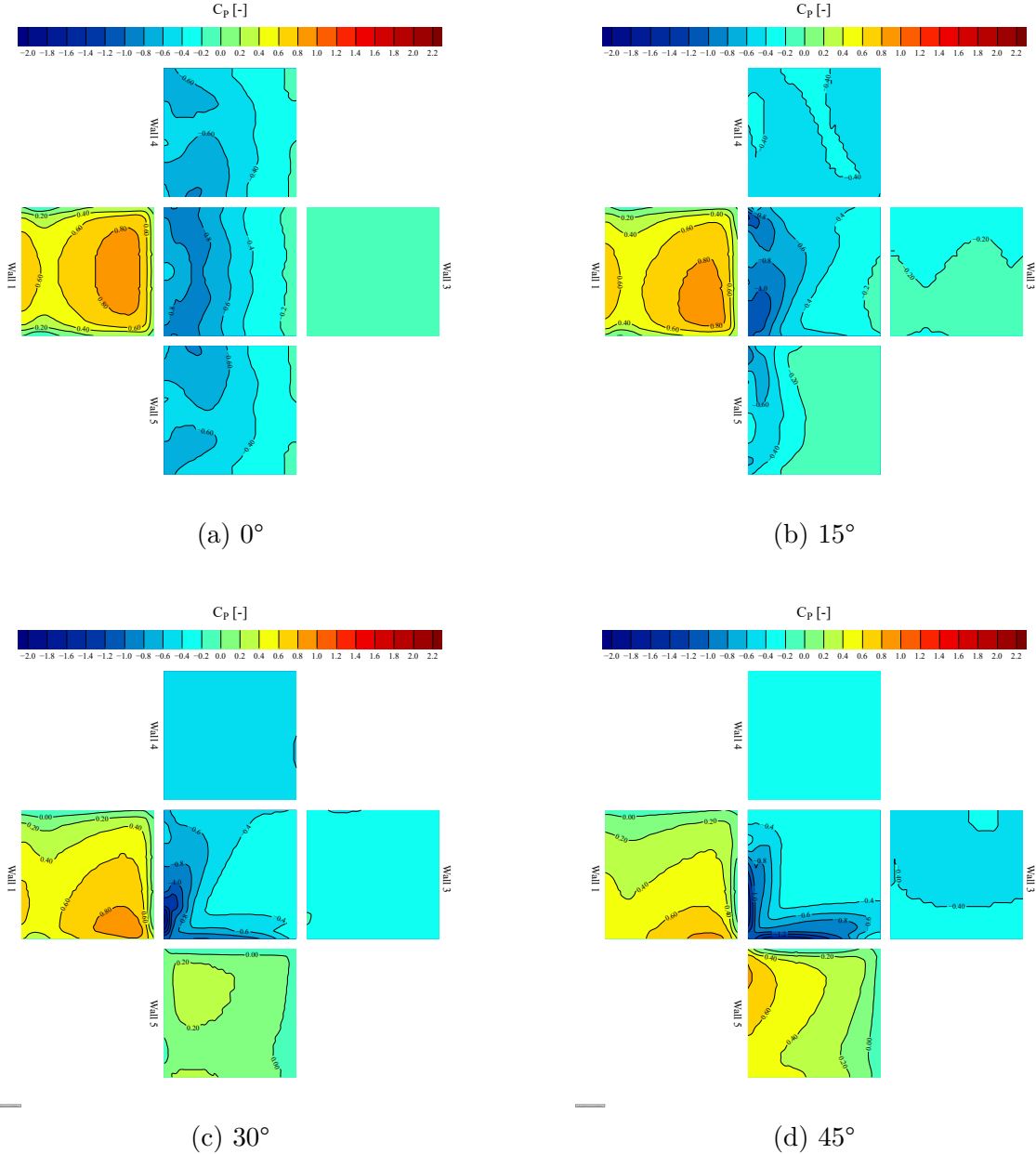


Figure 1.10: C_P contour maps, SST $k\omega$

1.3 Quantitative analysis of wall-averaged pressure coefficient $\overline{C_P}$

Table 1.1 presents the averaged pressure coefficient ($\overline{C_P}$) over the entire surface, based on the available database information and the studied $k\text{-}\epsilon$ and $k\text{-}\omega$ turbulence models.

Table 1.2 presents the relative error (ε_r), calculated using Equation 1.1, based on the values from Table 1.1.

$$\varepsilon_r = 100 \left| \frac{\varphi_{(x=0)} - \varphi_{(x)}}{\varphi_{(x=0)}} \right| \quad (1.1)$$

where $\varphi_{(x=0)}$ represents the *reference value*, and $\varphi_{(x)}$ denotes the *computed value*.

For the calculation of ε_r in Table 1.2, the AIVC dataset was used as the reference value $\varphi_{(x=0)}$.

Yellow and green cells indicate the smallest and second smallest ε_r values, respectively, for the turbulence models. The BDA and TPU ε_r values are included as reference.

Following the same methodology as in Table 1.2, Tables 1.3 and 1.4 present the smallest and second smallest wall-averaged pressure coefficient ($\overline{C_P}$) relative error (ε_r) for the studied turbulence models, considering the BDA and TPU databases as reference values, respectively.

Table 1.1: Comparison of $\overline{C_P}$ on the walls. Databases, $k-\epsilon$ and $k-\omega$ turbulence models

Database / Model	Wind incidence	Wall 1	Wall 2	Wall 3	Wall 4	Wall 5
AIVC	0°	0.70	-	-0.20	-0.50	-0.50
BDA	0°	0.73	-0.74	-0.31	-0.65	-0.69
TPU	0°	0.68	-0.84	-0.35	-0.77	-0.75
$k-\epsilon$ STD	0°	0.69	-0.44	-0.18	-0.41	-0.41
$k-\epsilon$ Realizable	0°	0.64	-0.44	-0.17	-0.41	-0.41
$k-\epsilon$ RNG	0°	0.64	-0.47	-0.22	-0.44	-0.44
$k-\omega$ STD	0°	0.74	-0.43	-0.18	-0.40	-0.40
$k-\omega$ SST	0°	0.58	-0.53	-0.16	-0.47	-0.47
TPU	15°	0.63	-0.74	-0.36	-0.74	-0.37
$k-\epsilon$ STD	15°	0.67	-0.48	-0.22	-0.46	-0.18
$k-\epsilon$ Realizable	15°	0.63	-0.48	-0.22	-0.42	-0.19
$k-\epsilon$ RNG	15°	0.62	-0.52	-0.27	-0.55	-0.19
$k-\omega$ STD	15°	0.72	-0.46	-0.22	-0.44	-0.17
$k-\omega$ SST	15°	0.56	-0.52	-0.21	-0.43	-0.22
BDA	30°	0.61	-0.72	-0.49	-0.72	0.01
TPU	30°	0.53	-0.70	-0.44	-0.70	0.10
$k-\epsilon$ STD	30°	0.58	-0.52	-0.28	-0.48	0.14
$k-\epsilon$ Realizable	30°	0.55	-0.51	-0.27	-0.44	0.13
$k-\epsilon$ RNG	30°	0.55	-0.56	-0.34	-0.53	0.13
$k-\omega$ STD	30°	0.62	-0.51	-0.27	-0.46	0.16
$k-\omega$ SST	30°	0.48	-0.51	-0.26	-0.46	0.10
AIVC	45°	0.35	-	-0.40	-0.40	0.35
BDA	45°	0.40	-0.71	-0.61	-0.60	0.32
TPU	45°	0.33	-0.63	-0.52	-0.53	0.34
$k-\epsilon$ STD	45°	0.43	-0.49	-0.35	-0.35	0.43
$k-\epsilon$ Realizable	45°	0.40	-0.49	-0.31	-0.31	0.40
$k-\epsilon$ RNG	45°	0.40	-0.54	-0.41	-0.41	0.40
$k-\omega$ STD	45°	0.45	-0.49	-0.32	-0.32	0.45
$k-\omega$ SST	45°	0.36	-0.49	-0.41	-0.26	0.32

Table 1.2: Wall $\overline{C_P}$ relative error with respect to AIVC database

Database / Turbulence model	Wind incidence	Wall 1 [%]	Wall 2 [%]	Wall 3 [%]	Wall 4 [%]	Wall 5 [%]
AIVC	0°	*	*	*	*	*
BDA	0°	4.29	*	55.00	30.00	38.00
TPU	0°	2.86	*	75.00	54.00	50.00
$k-\epsilon$ STD	0°	1.43	*	10.00	18.00	18.00
$k-\epsilon$ Realizable	0°	8.57	*	15.00	18.00	18.00
$k-\epsilon$ RNG	0°	8.57	*	10.00	12.00	12.00
$k-\omega$ STD	0°	5.71	*	10.00	20.00	20.00
$k-\omega$ SST	0°	17.14	*	20.00	6.00	6.00
AIVC	45°	*	*	*	*	*
BDA	45°	14.29	*	52.50	50.00	8.57
TPU	45°	5.71	*	30.00	32.50	2.86
$k-\epsilon$ STD	45°	22.86	*	12.50	12.50	22.86
$k-\epsilon$ Realizable	45°	14.29	*	22.50	22.50	14.29
$k-\epsilon$ RNG	45°	14.29	*	2.50	2.50	14.29
$k-\omega$ STD	45°	28.57	*	20.00	20.00	28.57
$k-\omega$ SST	45°	2.86	*	2.50	35.00	8.57

Table 1.3: Wall $\overline{C_P}$ relative error with respect to BDA database

Turbulence model	Wind incidence	Wall 1 [%]	Wall 2 [%]	Wall 3 [%]	Wall 4 [%]	Wall 5 [%]
$k-\epsilon$ STD	0°	10.96	37.84	41.94	36.92	40.58
$k-\epsilon$ Realizable	0°	17.81	37.84	45.16	36.92	40.58
$k-\epsilon$ RNG	0°	19.18	33.78	25.81	27.69	31.88
$k-\omega$ STD	0°	1.37	37.84	41.94	38.46	42.03
$k-\omega$ SST	0°	26.03	29.73	48.39	29.23	33.33
$k-\epsilon$ STD	30°	6.56	25.00	40.82	33.33	1200.00
$k-\epsilon$ Realizable	30°	14.75	26.39	44.90	38.89	1000.00
$k-\epsilon$ RNG	30°	13.11	19.44	30.61	26.39	1000.00
$k-\omega$ STD	30°	0.00	26.39	44.90	36.11	1400.00
$k-\omega$ SST	30°	26.23	26.39	46.94	36.11	800.00
$k-\epsilon$ STD	45°	5.00	28.17	44.26	43.33	31.25
$k-\epsilon$ Realizable	45°	5.00	29.58	50.82	50.00	18.75
$k-\epsilon$ RNG	45°	5.00	21.13	32.79	31.67	18.75
$k-\omega$ STD	45°	12.50	28.17	49.18	48.33	40.63
$k-\omega$ SST	45°	12.50	29.58	32.79	56.67	3.13

Table 1.4: Wall $\overline{C_P}$ relative error with respect to TPU database

Turbulence model	Wind incidence	Wall 1 [%]	Wall 2 [%]	Wall 3 [%]	Wall 4 [%]	Wall 5 [%]
$k-\epsilon$ STD	0°	8.82	50.00	48.57	46.75	45.33
$k-\epsilon$ Realizable	0°	1.47	48.81	51.43	48.05	46.67
$k-\epsilon$ RNG	0°	1.47	45.24	34.29	41.56	40.00
$k-\omega$ STD	0°	17.65	50.00	48.57	48.05	46.67
$k-\omega$ SST	0°	10.29	35.71	54.29	38.96	37.33
$k-\epsilon$ STD	15°	14.29	39.19	38.89	37.84	54.05
$k-\epsilon$ Realizable	15°	6.35	37.84	41.67	43.24	51.35
$k-\epsilon$ RNG	15°	6.35	33.78	25.00	25.68	51.35
$k-\omega$ STD	15°	23.81	40.54	41.67	40.54	54.05
$k-\omega$ SST	15°	6.35	29.73	41.67	41.89	40.54
$k-\epsilon$ STD	30°	16.98	31.43	36.36	31.43	60.00
$k-\epsilon$ Realizable	30°	9.43	31.43	38.64	37.14	40.00
$k-\epsilon$ RNG	30°	9.43	25.71	22.73	24.29	40.00
$k-\omega$ STD	30°	24.53	31.43	38.64	34.29	70.00
$k-\omega$ SST	30°	3.77	30.00	40.91	34.29	10.00
$k-\epsilon$ STD	45°	36.36	26.98	34.62	35.85	32.35
$k-\epsilon$ Realizable	45°	27.27	26.98	40.38	41.51	20.59
$k-\epsilon$ RNG	45°	27.27	20.63	21.15	22.64	20.59
$k-\omega$ STD	45°	42.42	26.98	40.38	39.62	38.24
$k-\omega$ SST	45°	15.15	28.57	21.15	52.83	0.00

Chapter 2

Local CFD Pressure Coefficient Comparison with BDA and TPU Databases

Since the BDA and TPU databases provide tap coordinates and C_P values, it is possible to perform a *local* comparison for each tap position, even though the experimental and CFD cases were conducted at different scales. Figure 2.1 shows the experimental pressure tap positions for the BDA and TPU studies. In the BDA study, 125 pressure taps were used, with 25 taps arranged equidistantly on each wall (Figure 2.1a). In contrast, the TPU study used 284 pressure taps, with wall 2 having 64 equidistant taps, while the other walls had 55 taps arranged in a specific pattern, as shown in Figure 2.1b.

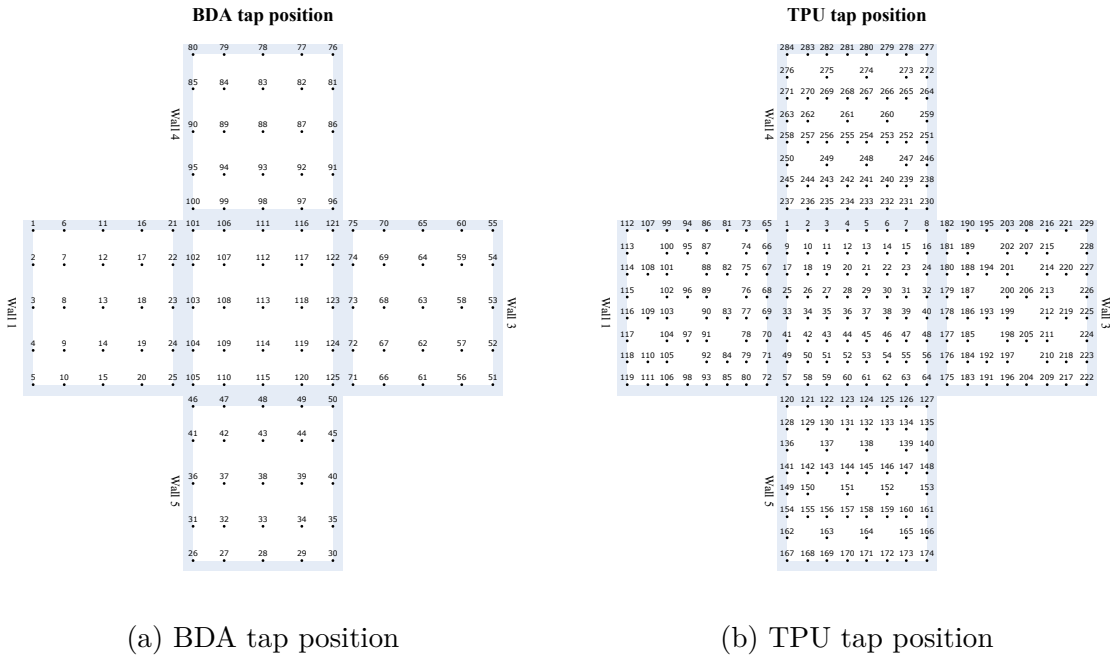


Figure 2.1: Experimental BDA and TPU tap position

Section 2.1 presents the contour maps derived from the experimental data of the BDA database, along with the corresponding CFD contour maps at the pressure tap coordinates provided by the database. Section 2.2 presents a similar set of contour maps for the TPU database.

Section 2.3 evaluates the accuracy of the turbulence models by comparing them with experimental data from the BDA and TPU databases. The analysis considers all walls, the wind incidence angles available from experimental observations, and all turbulence models tested in this study.

Section 2.4 presents a qualitative analysis of the local pressure coefficients along the horizontal and vertical center-lines of the building. The analysis considers wind incidence angles of 0° , 15° , 30° , and 45° , and the results are compared with experimental data from the BDA and TPU datasets.

Section 2.5 presents the turbulent kinetic energy and turbulent viscosity fields on parallel and cross-sectional planes relative to the ABL angle of attack.

Section 2.6 qualitatively compares the streamlines in the top view, formed by the wind flow at 0° , 15° , 30° , and 45° for all the turbulence models studied. The objective is to identify differences in the recirculation and flow separation patterns for each turbulence model.

2.1 Pressure Coefficient Contour Maps. BDA vs CFD

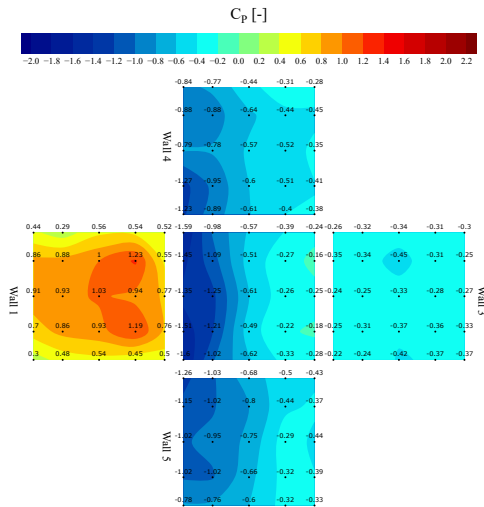


Figure 2.2: C_P contour maps, BDA 0°

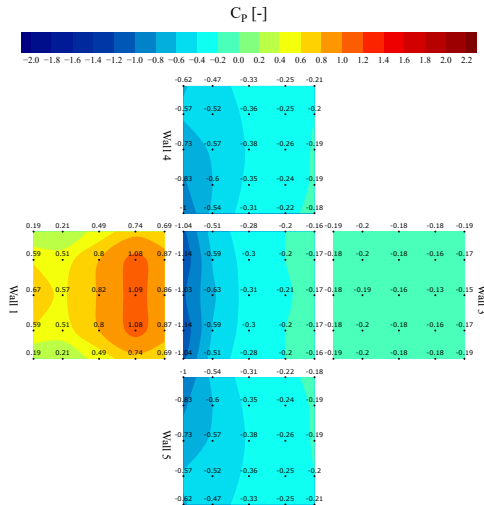


Figure 2.3: C_P contour maps at BDA tap coordinates, STD $k-\epsilon$, 0°

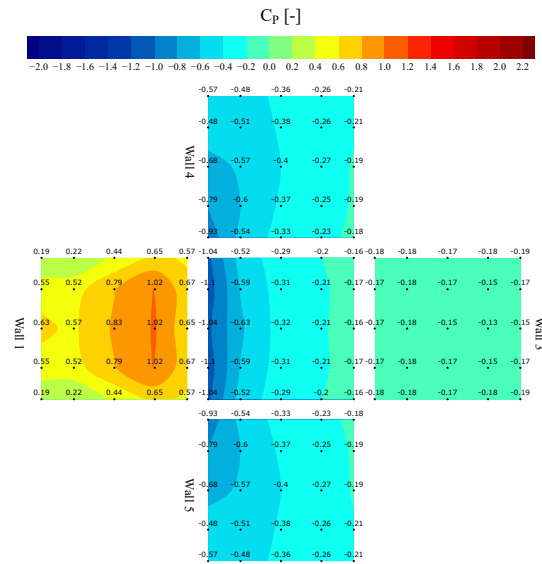


Figure 2.4: C_P contour maps at BDA tap coordinates, Realizable $k-\epsilon$, 0°

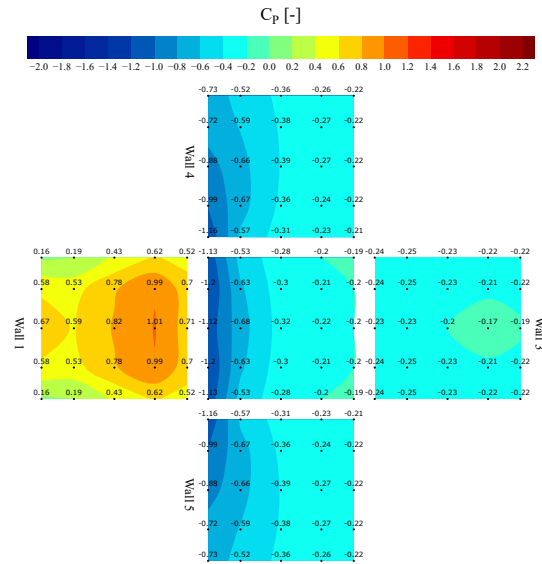


Figure 2.5: C_P contour maps at BDA tap coordinates, RNG $k-\epsilon$, 0°

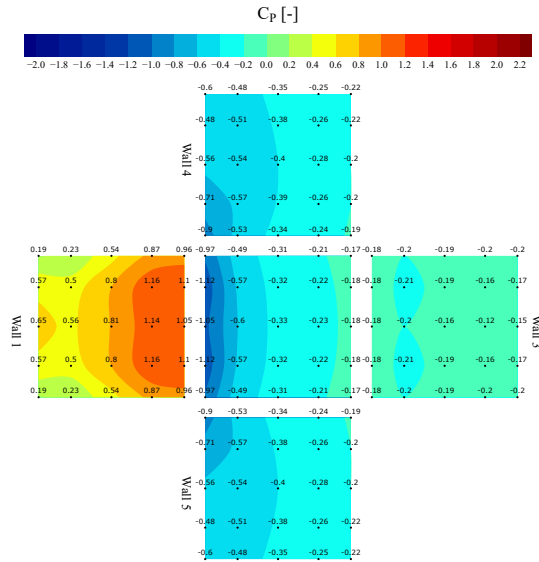


Figure 2.6: C_P contour maps at BDA tap coordinates, STD $k-\omega$, 0°

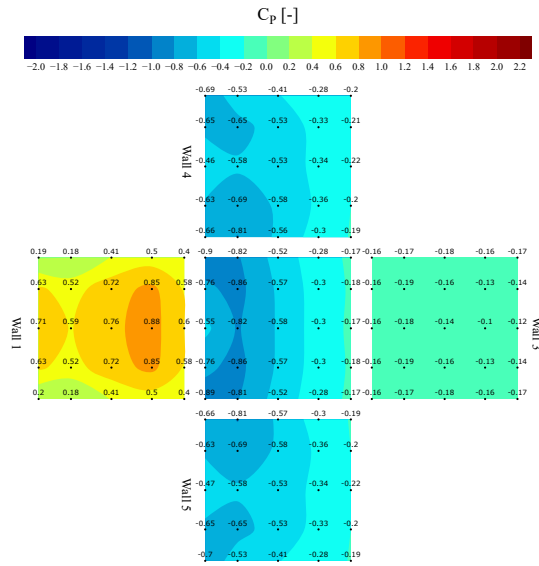


Figure 2.7: C_P contour maps at BDA tap coordinates, SST $k-\omega$, 0°

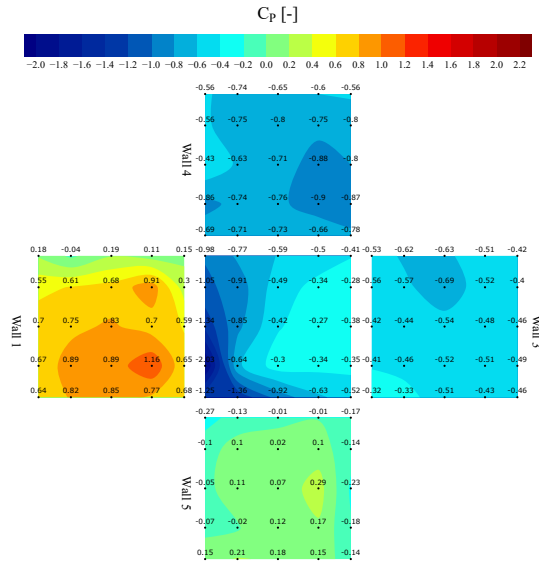


Figure 2.8: C_P contour maps, BDA 30°

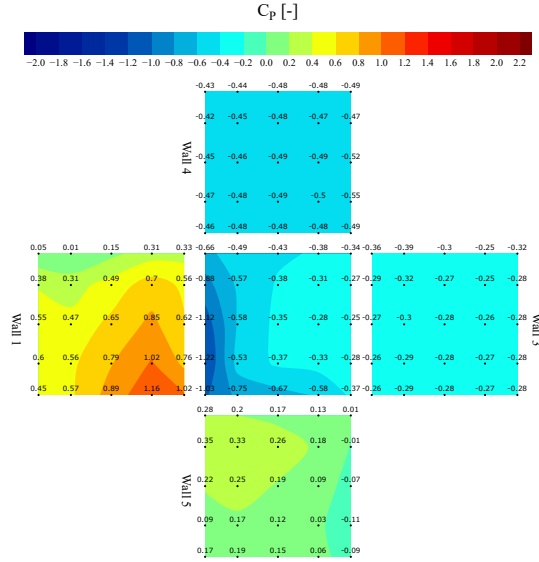


Figure 2.9: C_P contour maps at BDA tap coordinates, STD $k-\epsilon$, 30°

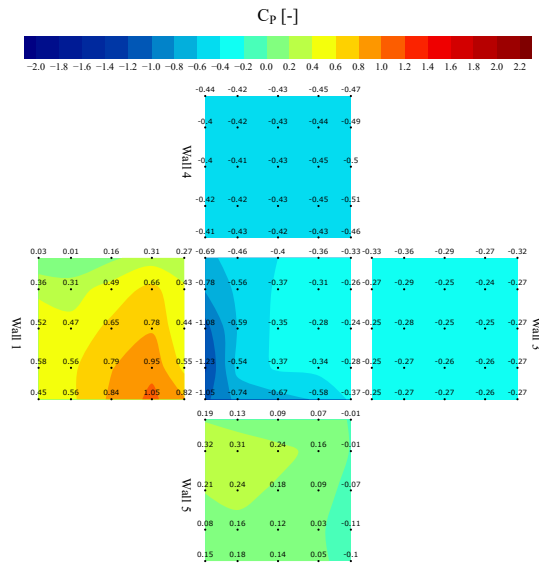


Figure 2.10: C_P contour maps at BDA tap coordinates, Realizable $k-\epsilon$, 30°

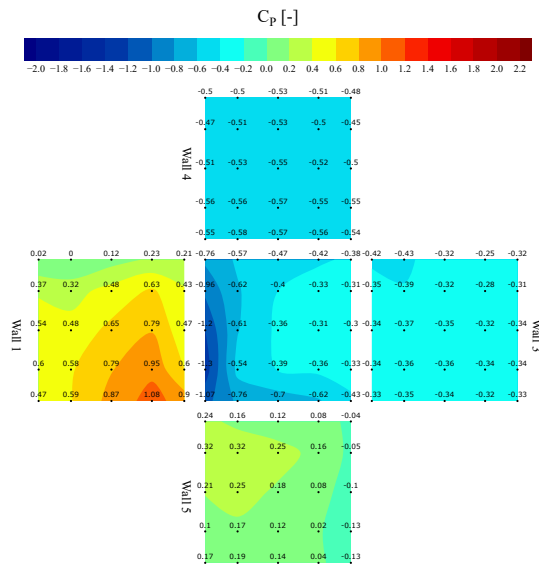


Figure 2.11: C_P contour maps at BDA tap coordinates, RNG $k-\epsilon$, 30°

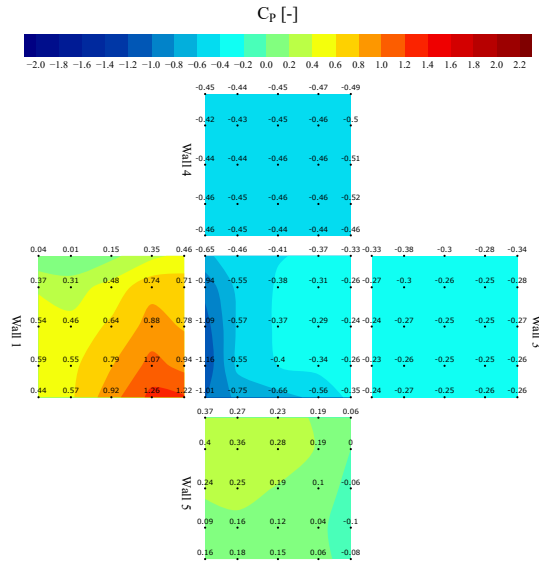


Figure 2.12: C_P contour maps at BDA tap coordinates, STD $k-\omega$, 30°

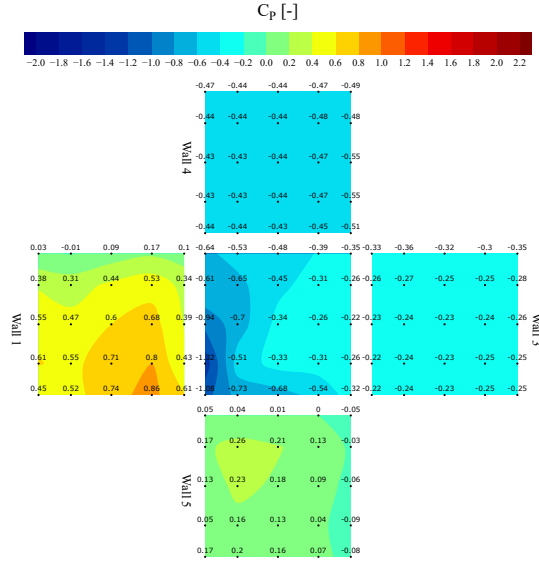


Figure 2.13: C_P contour maps at BDA tap coordinates, SST $k-\omega$, 30°

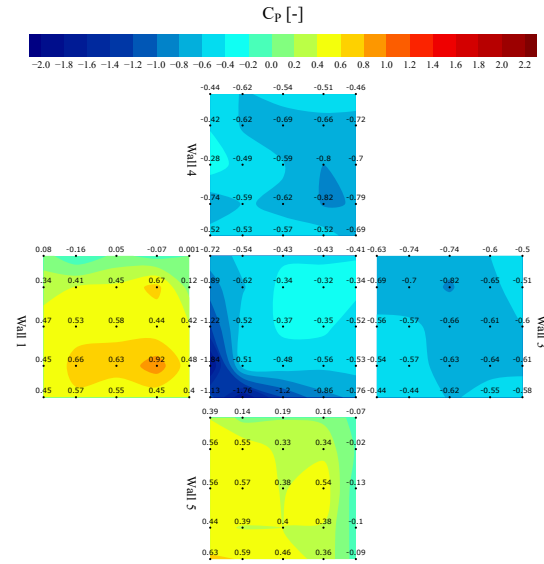


Figure 2.14: C_P contour maps, BDA 45°

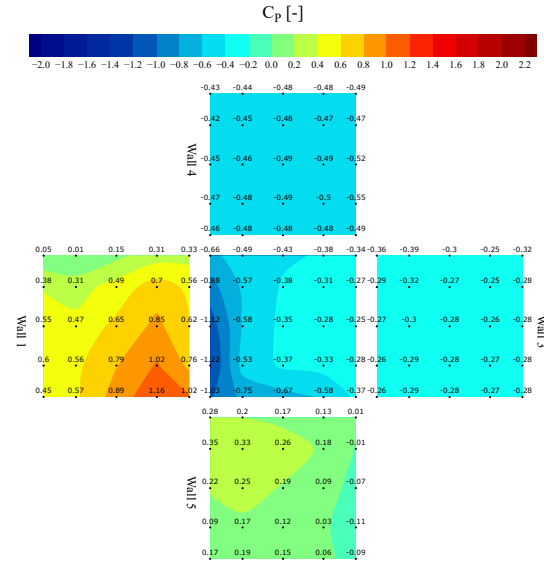


Figure 2.15: C_P contour maps at BDA tap coordinates, STD $k-\epsilon$, 45°

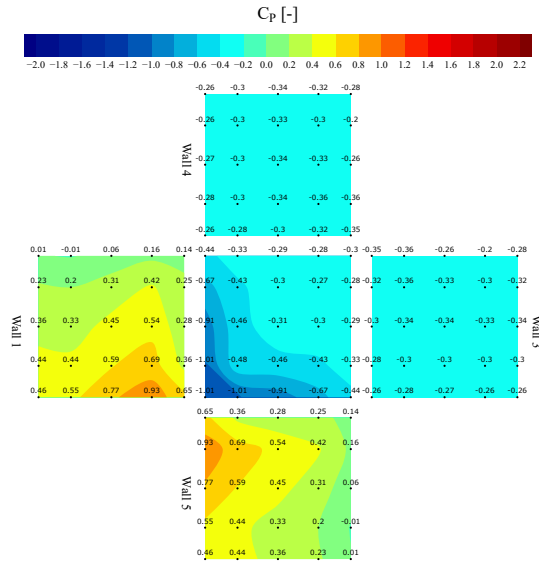


Figure 2.16: C_P contour maps at BDA tap coordinates, Realizable $k-\epsilon$, 45°

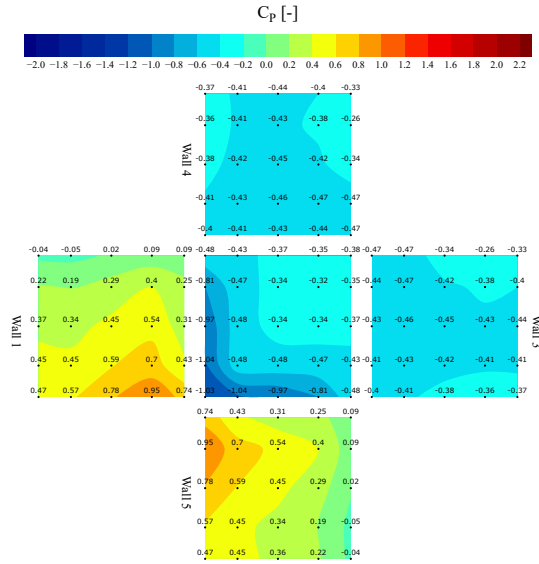


Figure 2.17: C_P contour maps at BDA tap coordinates, RNG $k-\epsilon$, 45°

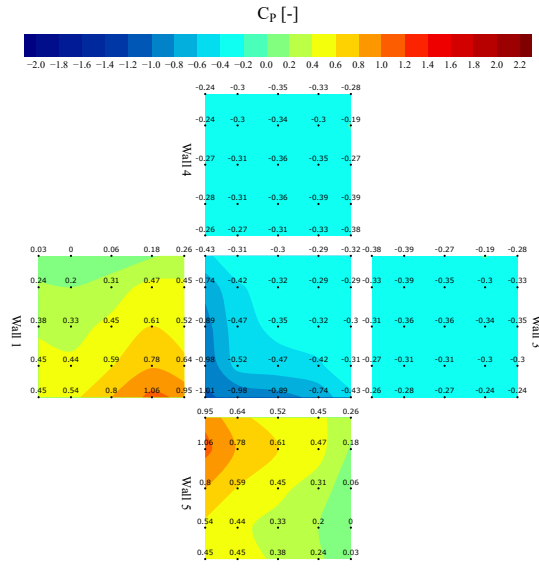


Figure 2.18: C_P contour maps at BDA tap coordinates, STD $k-\omega$, 45°

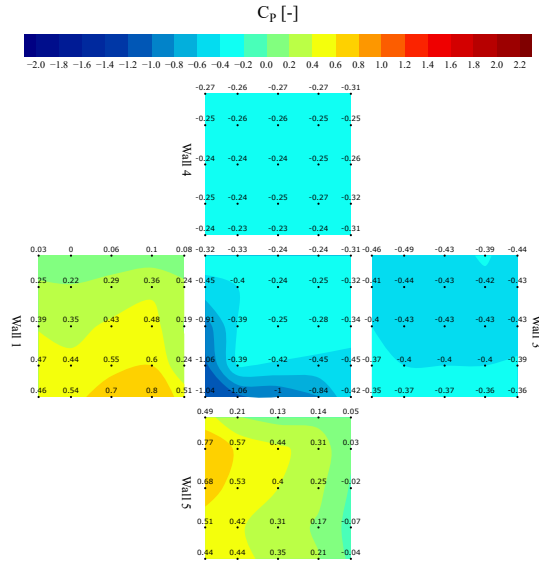


Figure 2.19: C_P contour maps at BDA tap coordinates, SST $k-\omega$, 45°

2.2 Pressure Coefficient Contour Maps. TPU vs CFD

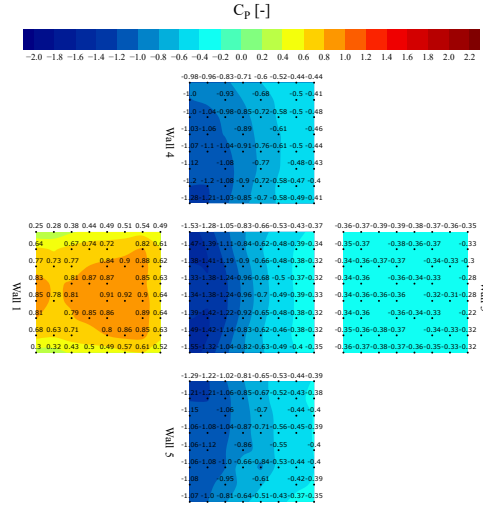


Figure 2.20: C_P contour maps, TPU 0°

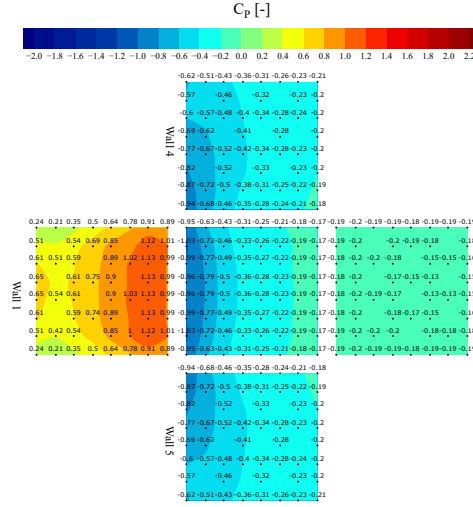


Figure 2.21: C_P contour maps at TPU tap coordinates, STD $k-\epsilon$, 0°

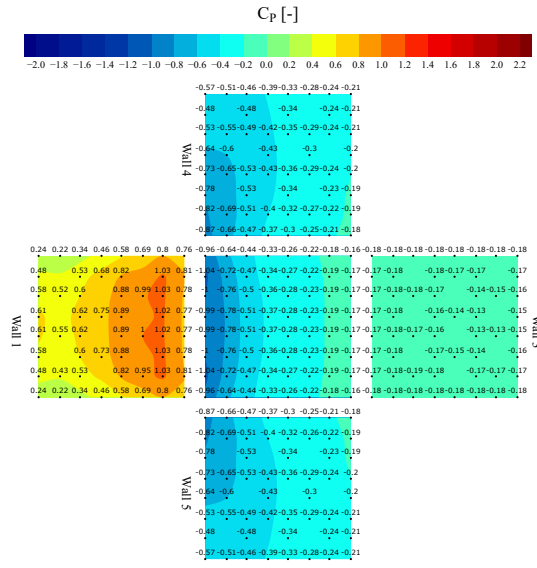


Figure 2.22: C_P contour maps at TPU tap coordinates, Realizable $k-\epsilon$, 0°

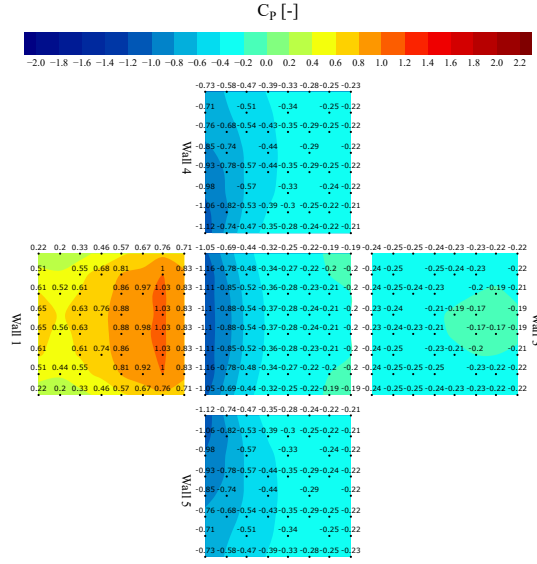


Figure 2.23: C_P contour maps at TPU tap coordinates, RNG $k-\epsilon$, 0°

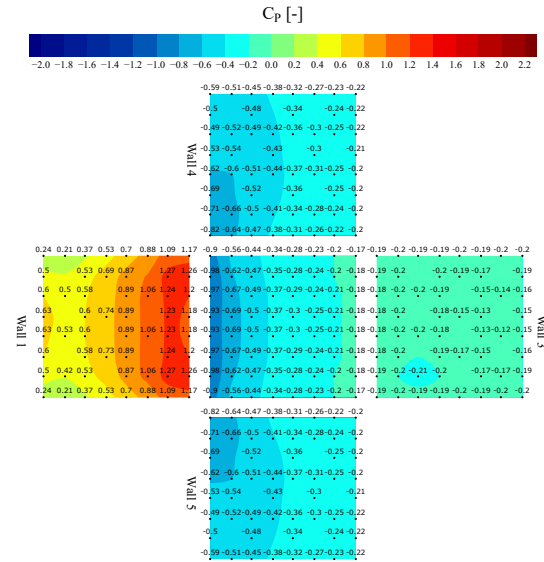


Figure 2.24: C_P contour maps at TPU tap coordinates, STD $k-\omega$, 0°

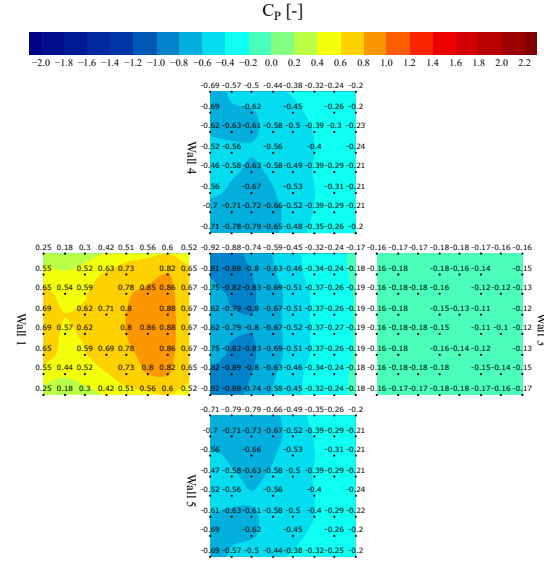


Figure 2.25: C_P contour maps at TPU tap coordinates, SST $k-\omega$, 0°

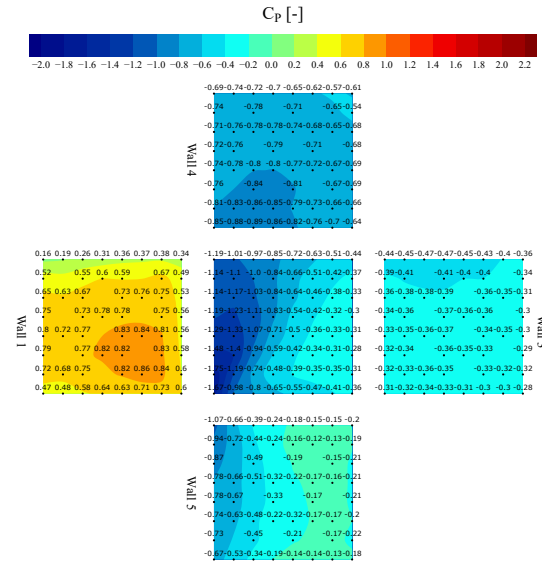


Figure 2.26: C_P contour maps, TPU 15°

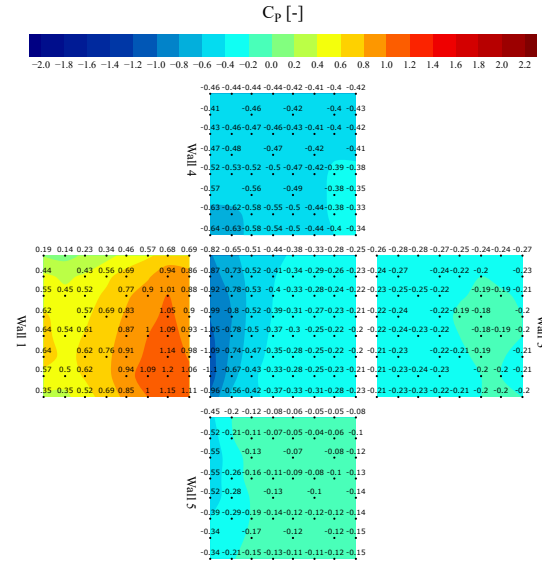


Figure 2.27: C_P contour maps at TPU tap coordinates, STD $k-\epsilon$, 15°

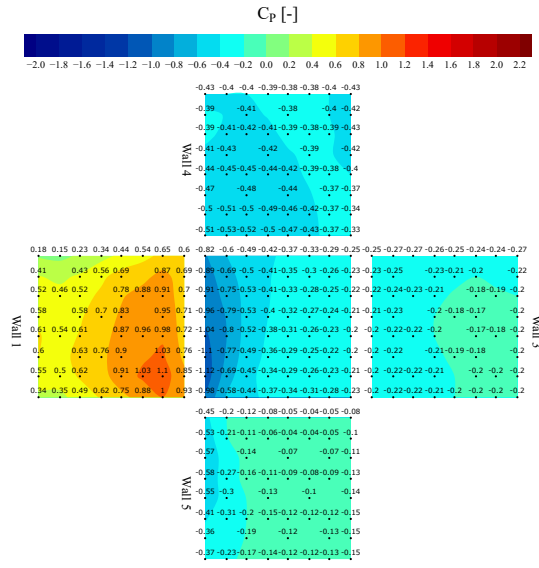


Figure 2.28: C_P contour maps at TPU tap coordinates, Realizable $k-\epsilon$, 15°

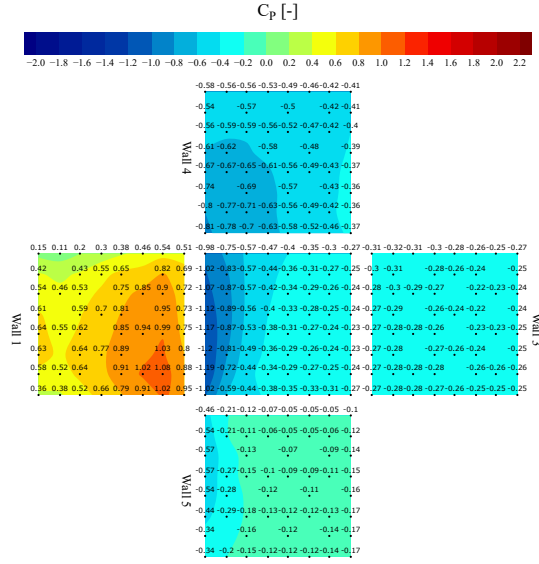


Figure 2.29: C_P contour maps at TPU tap coordinates, RNG $k-\epsilon$, 15°

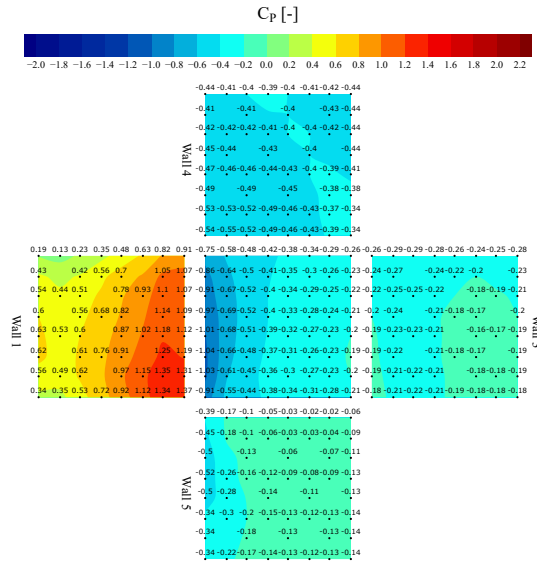


Figure 2.30: C_P contour maps at TPU tap coordinates, STD $k-\omega$, 15°

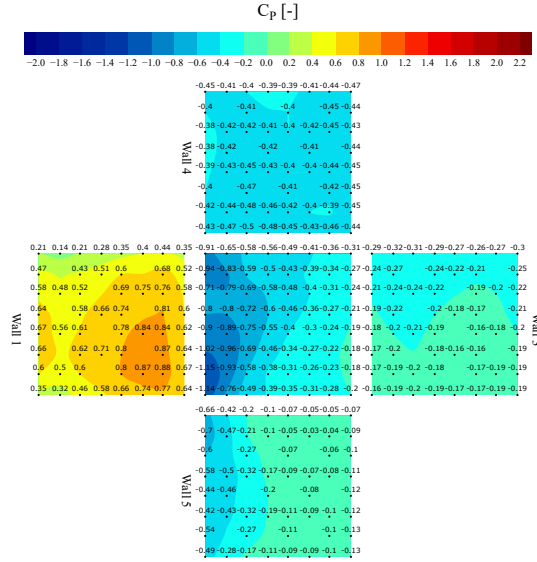


Figure 2.31: C_P contour maps at TPU tap coordinates, SST $k-\omega$, 15°

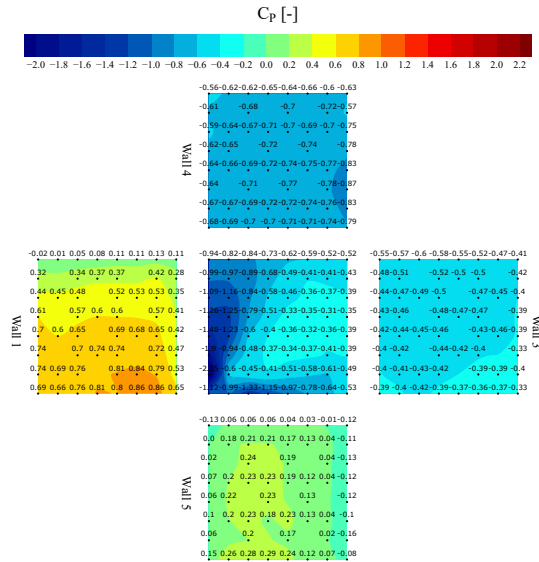


Figure 2.32: C_P contour maps, TPU 30°

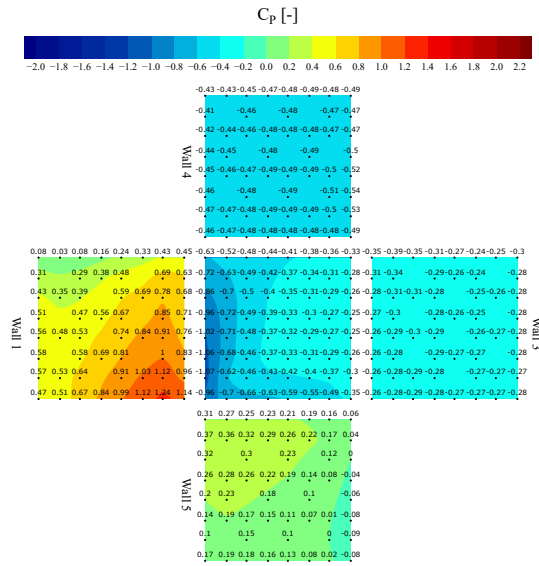


Figure 2.33: C_P contour maps at TPU tap coordinates, STD $k-\epsilon$, 30°

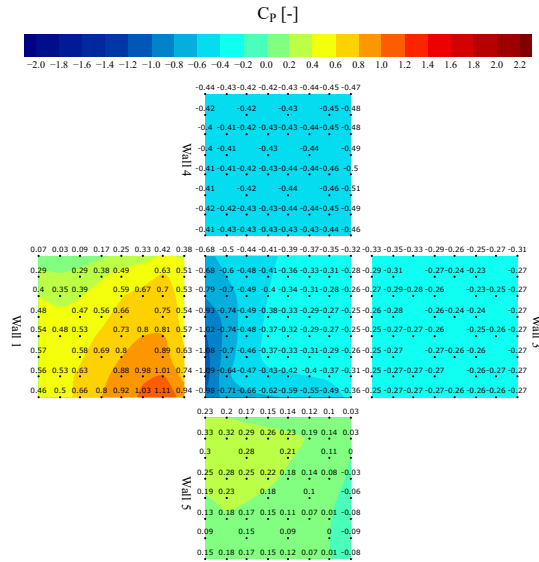


Figure 2.34: C_P contour maps at TPU tap coordinates, Realizable $k-\epsilon$, 30°

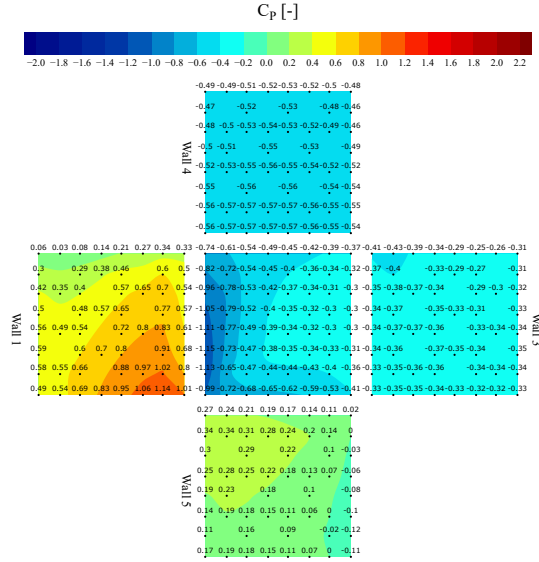


Figure 2.35: C_P contour maps at TPU tap coordinates, RNG $k-\epsilon$, 30°

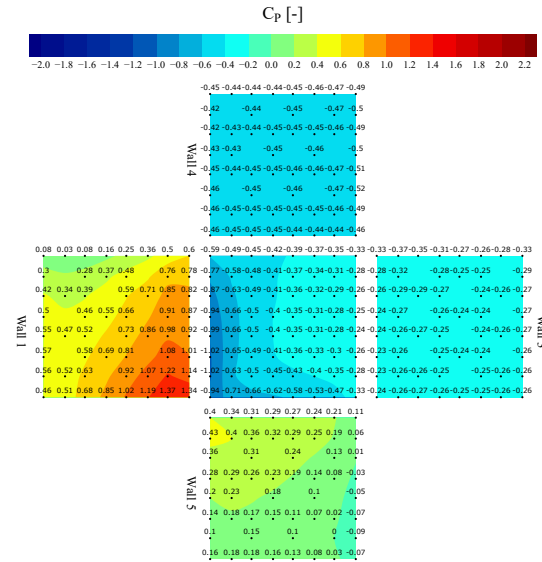


Figure 2.36: C_P contour maps at TPU tap coordinates, STD $k-\omega$, 30°

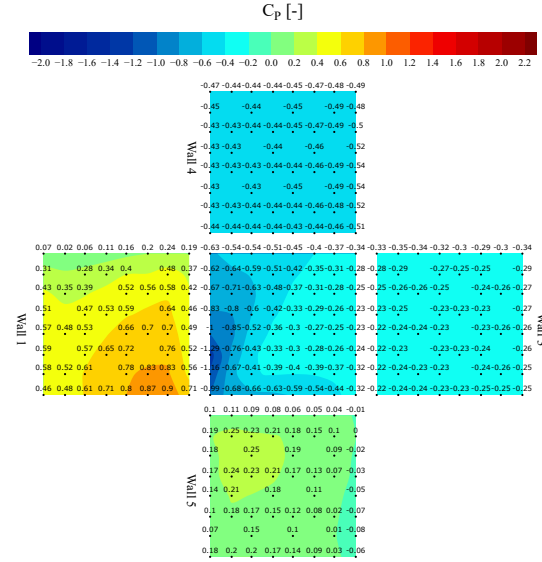


Figure 2.37: C_P contour maps at TPU tap coordinates, SST $k-\omega$, 30°

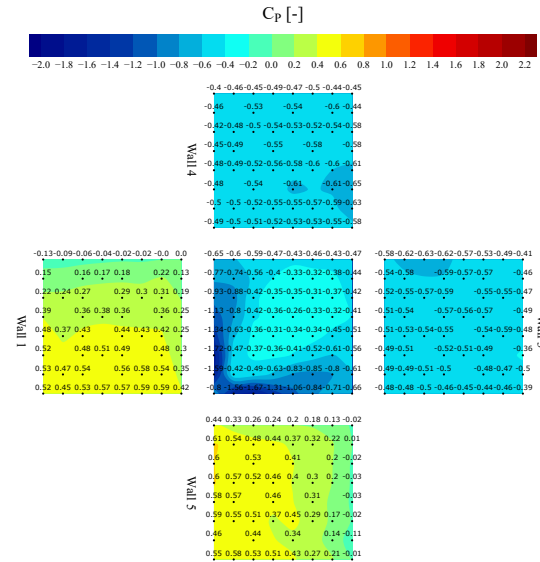


Figure 2.38: C_P contour maps, TPU 45°

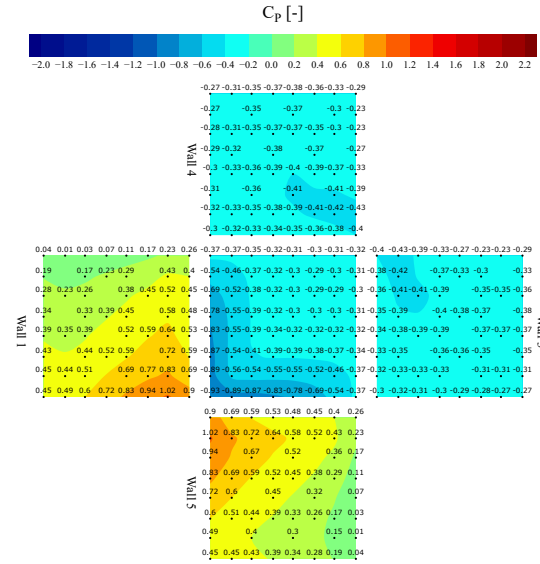


Figure 2.39: C_P contour maps at TPU tap coordinates, STD $k-\epsilon$, 45°

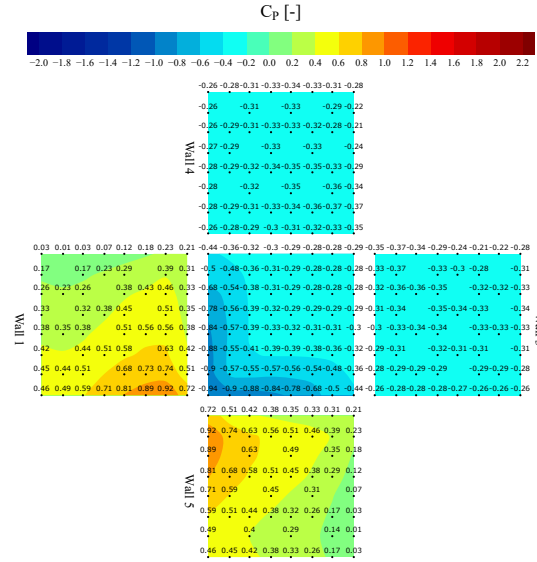


Figure 2.40: C_P contour maps at TPU tap coordinates, Realizable $k-\epsilon$, 45°

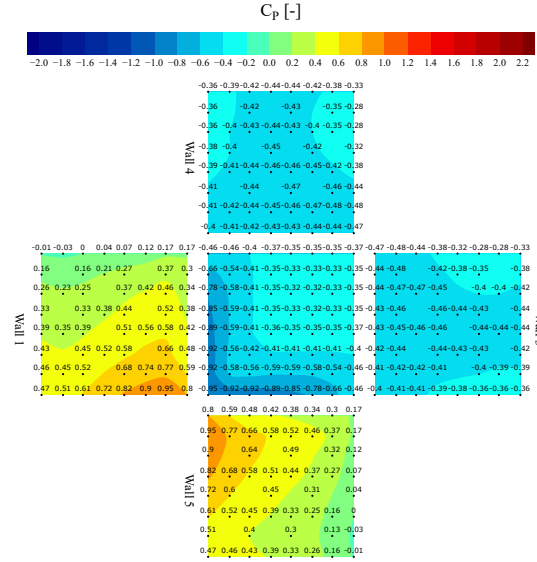


Figure 2.41: C_P contour maps at TPU tap coordinates, RNG $k-\epsilon$, 45°

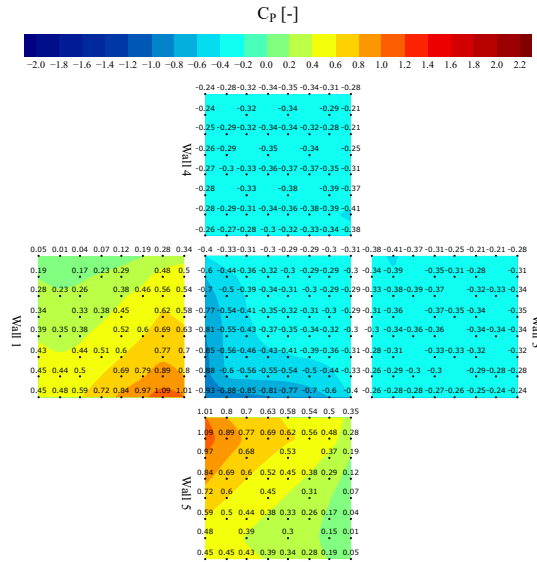


Figure 2.42: C_P contour maps at TPU tap coordinates, STD $k-\omega$, 45°

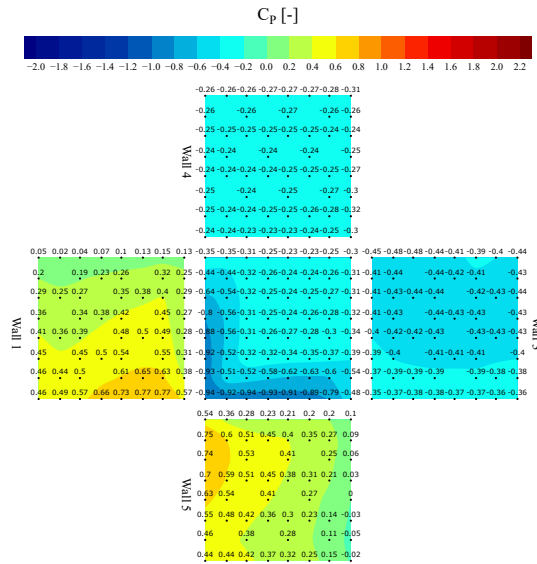


Figure 2.43: C_P contour maps at TPU tap coordinates, SST $k-\omega$, 45°

2.3 BDA and TPU Normalized Mean Square Error ($NMSE$) and Normalized Root Mean Square Error (ε)

To assess the accuracy of the turbulence models against data from the BDA (Figure 2.46) and TPU (Figure 2.47) databases, the Normalized Mean Square Error (NMSE) and Normalized Root Mean Square Error (ε) were computed for each wall and for all turbulence models (see Equations 2.1 and 2.2). NMSE quantifies the model's overall performance across the dataset. According to stringent validation criteria, an NMSE of zero indicates perfect agreement, while values below 1.5 are considered acceptable for accurate simulations. NMSE is defined as:

$$NMSE = \frac{\sum_{i=1}^n (y_i - \hat{y})^2}{\sum_{i=1}^n y_i \hat{y}} \quad (2.1)$$

Similarly, the normalized root mean square error (ε) is given by:

$$\varepsilon = \frac{\sqrt{\frac{\sum_{i=1}^n (y_i - \hat{y})^2}{n}}}{\bar{y}} \quad (2.2)$$

where y_i and \hat{y} are the observed and predicted C_P values at the i th tap position, respectively, n is the total number of taps on the wall, and \bar{y} is the mean wall C_P value.

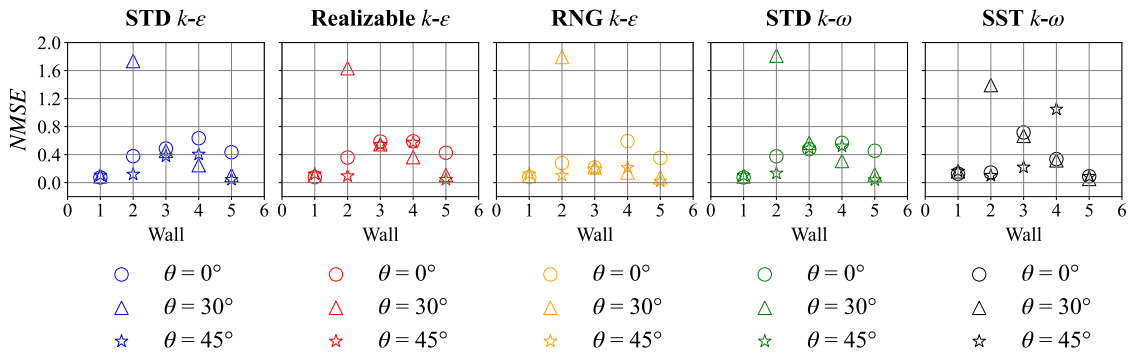


Figure 2.44: $NMSE$ referred to BDA basedata per wall for all turbulence models.

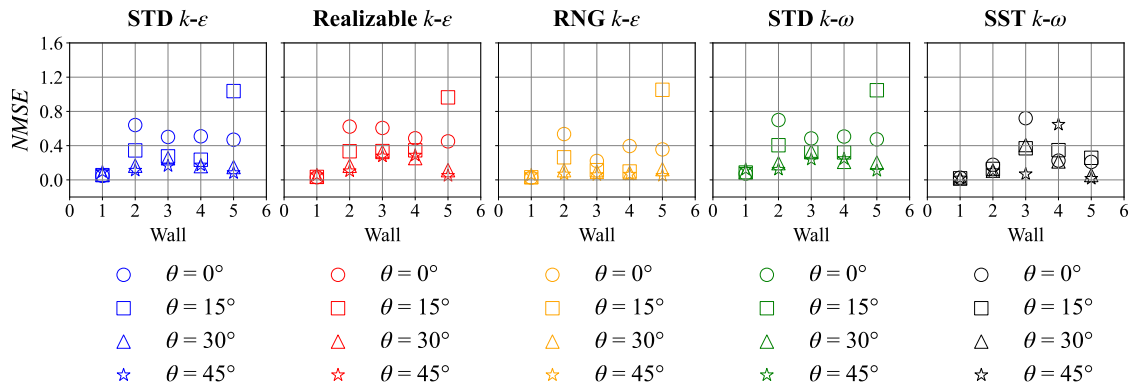


Figure 2.45: $NMSE$ referred to TPU basedata per wall for all turbulence models.

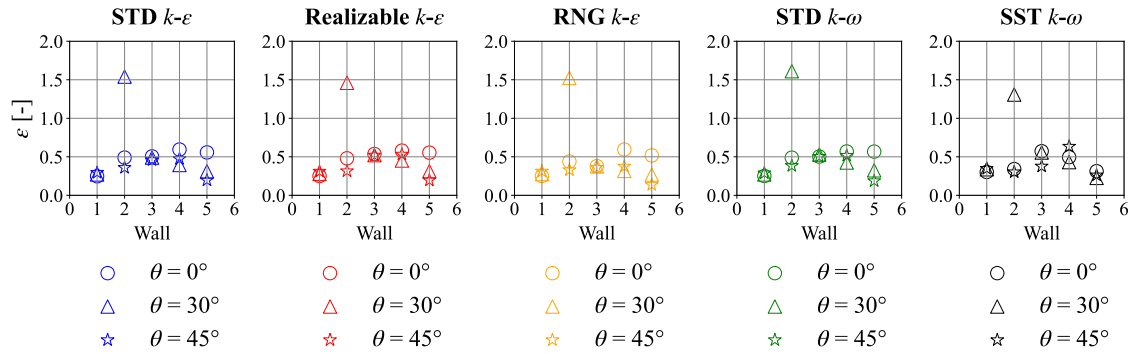


Figure 2.46: ε referred to BDA basedata per wall for all turbulence models.

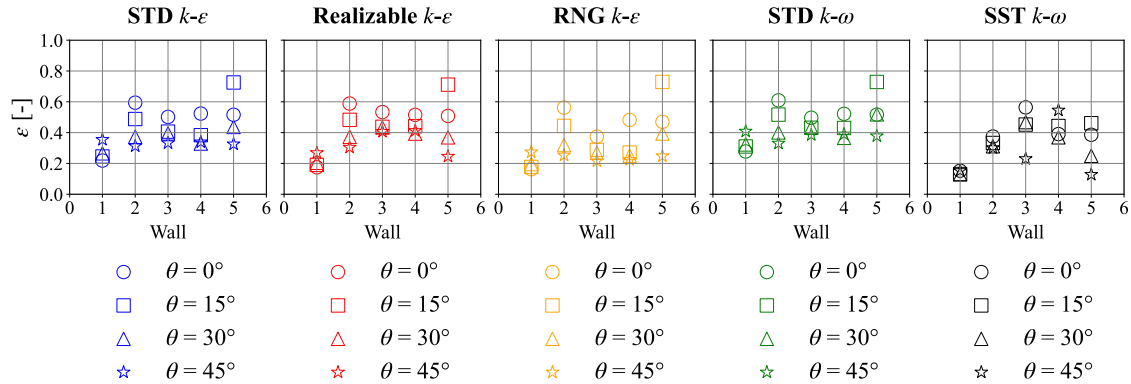


Figure 2.47: ε referred to TPU basedata per wall for all turbulence models.

2.4 Comparison Of Pressure Coefficients At Wall Center-lines With Respect To Databases

Figure 2.48 illustrates the relative positions of the pressure taps in the BDA and TPU experimental studies. For clarity, the blue line will henceforth be referred to as the “horizontal center-line”, and the red line as the “vertical center-line”.

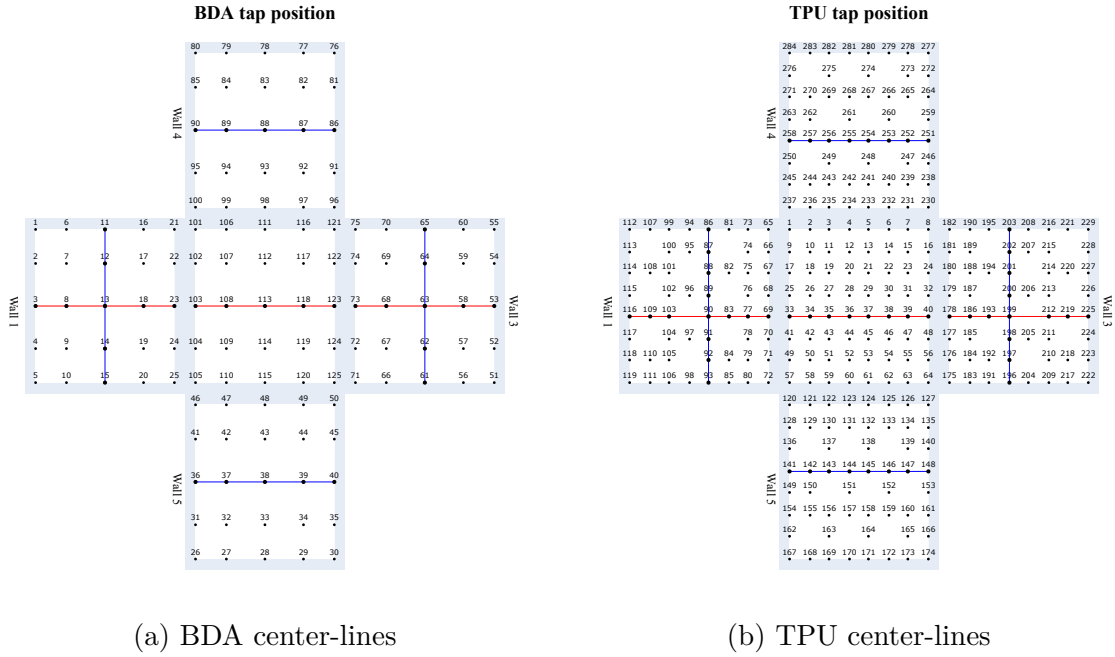
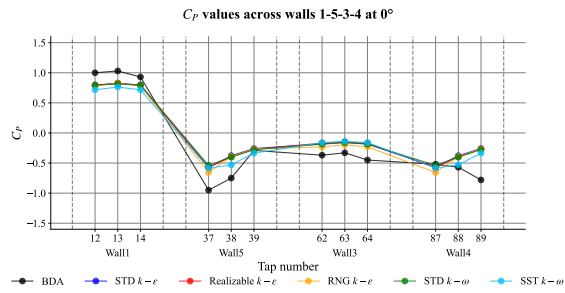
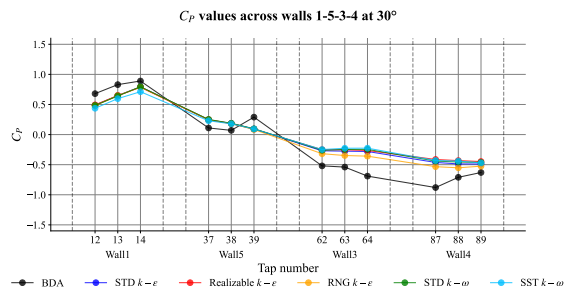


Figure 2.48: Center-lines at BDA and TPU tap position

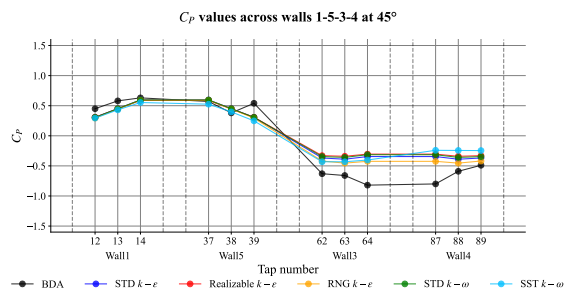
Figures 2.49 to 2.52 present the local pressure coefficients along the horizontal and vertical center-lines for wind incidence angles of 0° , 15° , 30° , and 45° . These results are compared with experimental data obtained from the BDA and TPU datasets.



(a) BDA C_P at horizontal center-line at 0°

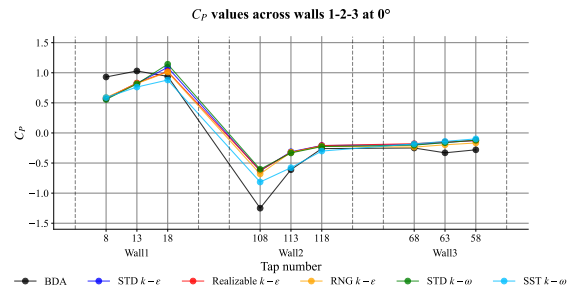


(b) BDA C_P at horizontal center-line at 30°

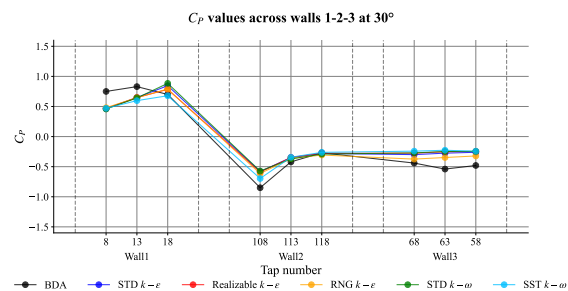


(c) BDA C_P at horizontal center-line at 45°

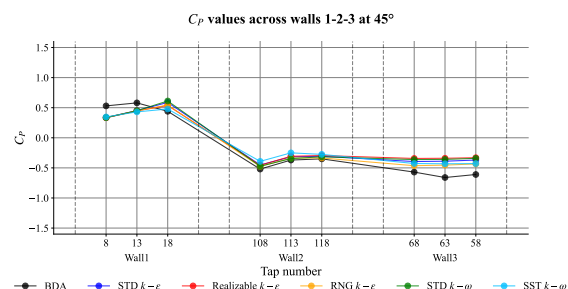
Figure 2.49: BDA C_P at horizontal center-line



(a) BDA C_P at vertical center-line at 0°

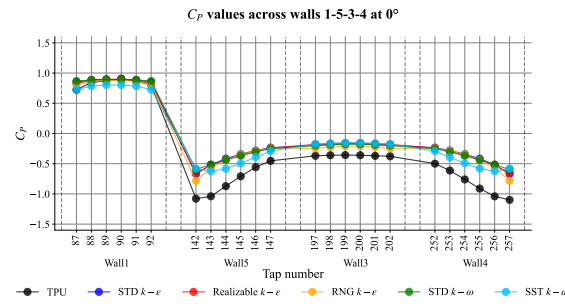


(b) BDA C_P at vertical center-line at 30°

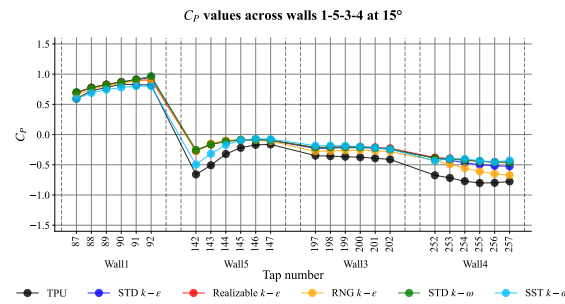


(c) BDA C_P at vertical center-line at 45°

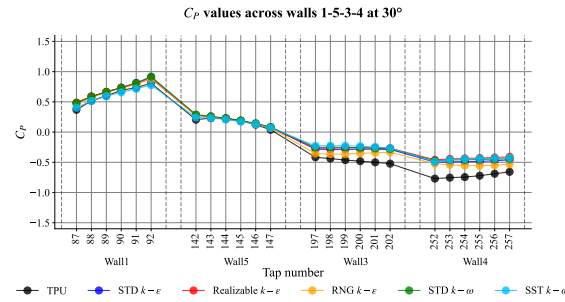
Figure 2.50: BDA C_P at vertical center-line



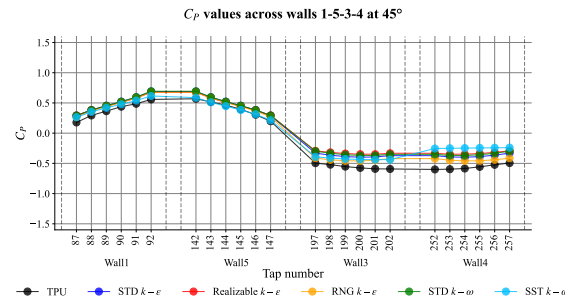
(a) TPU C_P at horizontal center-line at 0°



(b) TPU C_P at horizontal center-line at 15°

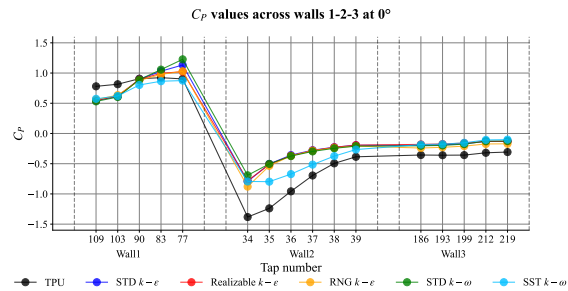


(c) TPU C_P at horizontal center-line at 30°

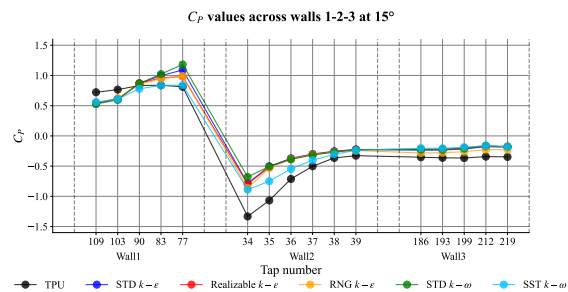


(d) TPU C_P at horizontal center-line at 45°

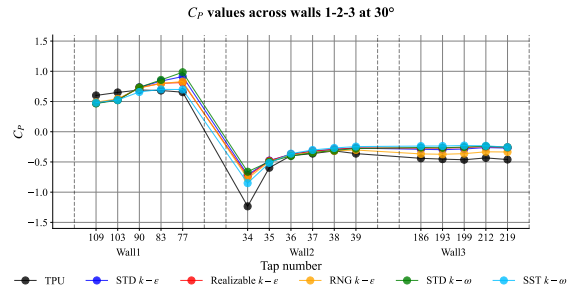
Figure 2.51: TPU C_P at horizontal center-line 57



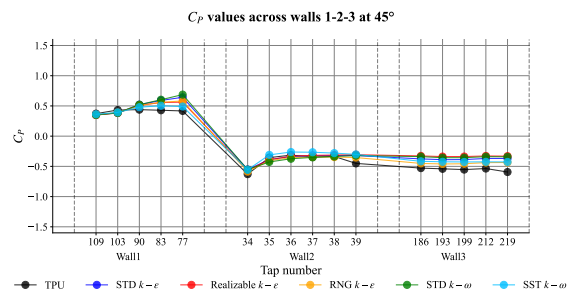
(a) TPU C_P at vertical center-line at 0°



(b) TPU C_P at vertical center-line at 15°



(c) TPU C_P at vertical center-line at 30°



(d) TPU C_P at vertical center-line at 45°

Figure 2.52: TPU C_P at vertical center-line
58

2.5 Turbulent Kinetic Energy and Turbulent Viscosity Fields in Parallel and Cross-Sectional Planes

Figures 2.54 to 2.68 present H/2 sections, oriented parallel and transverse to the flow, illustrating the turbulent viscosity variable for the studied turbulence models at wind incidence angles of 0°, 15°, 30°, and 45°.

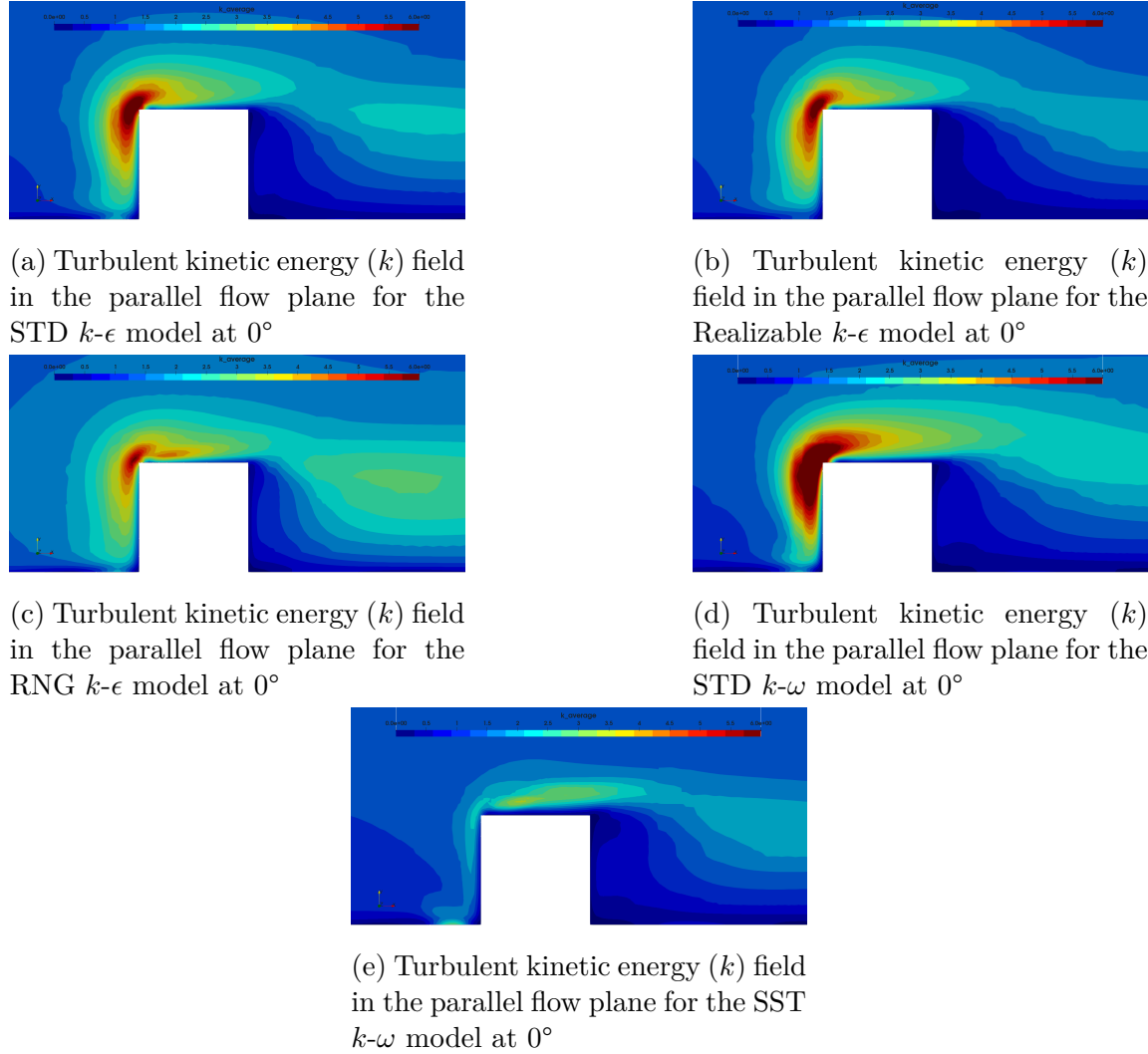
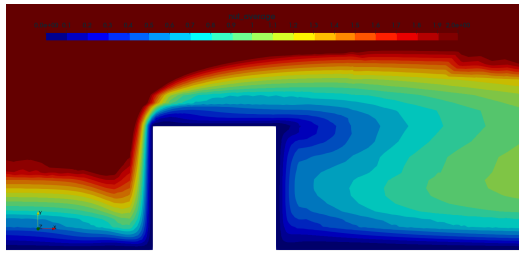
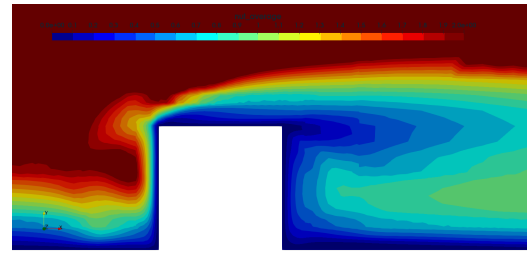


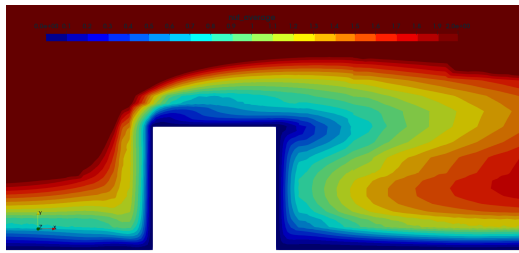
Figure 2.53: Turbulent kinetic energy (k) field in the parallel flow plane for turbulence models at 0°



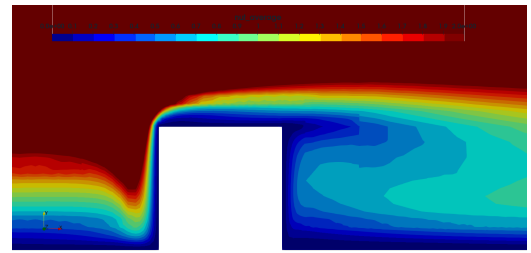
(a) Turbulent viscosity (ν_t) field in the parallel flow plane for the STD $k-\epsilon$ model at 0°



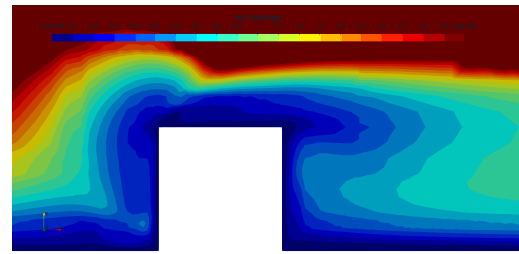
(b) Turbulent viscosity (ν_t) field in the parallel flow plane for the Realizable $k-\epsilon$ model at 0°



(c) Turbulent viscosity (ν_t) field in the parallel flow plane for the RNG $k-\epsilon$ model at 0°

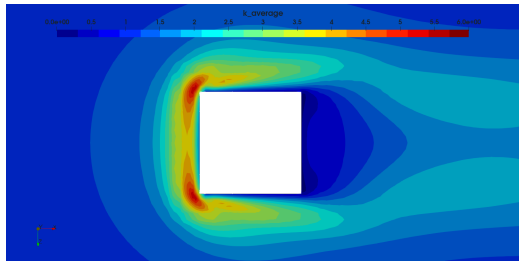


(d) Turbulent viscosity (ν_t) field in the parallel flow plane for the STD $k-\omega$ model at 0°

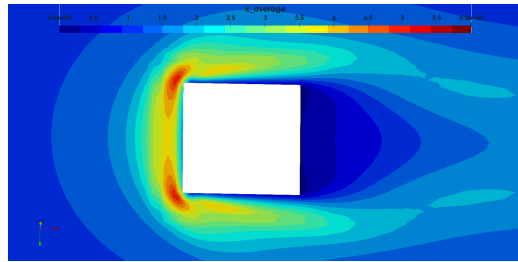


(e) Turbulent viscosity (ν_t) field in the parallel flow plane for the SST $k-\omega$ model at 0°

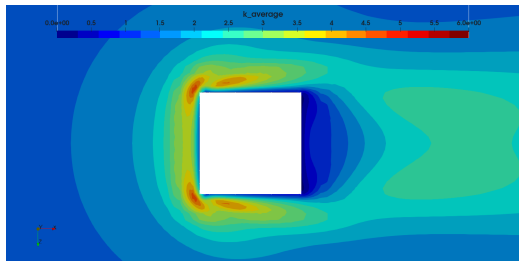
Figure 2.54: Turbulent viscosity (ν_t) field in the parallel flow plane for turbulence models at 0°



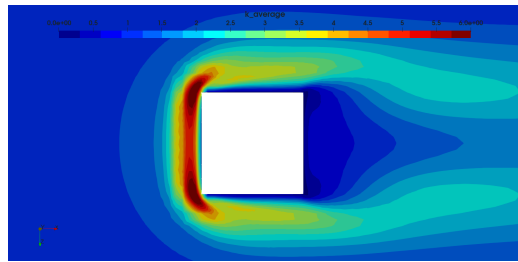
(a) Turbulent kinetic energy (k) field in the cross-sectional plane for the STD $k-\epsilon$ model at 0°



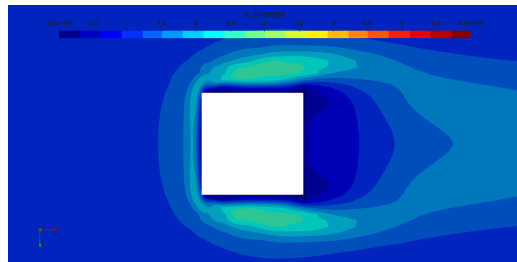
(b) Turbulent kinetic energy (k) field in the cross-sectional plane for the Realizable $k-\epsilon$ model at 0°



(c) Turbulent kinetic energy (k) field in the cross-sectional plane for the RNG $k-\epsilon$ model at 0°

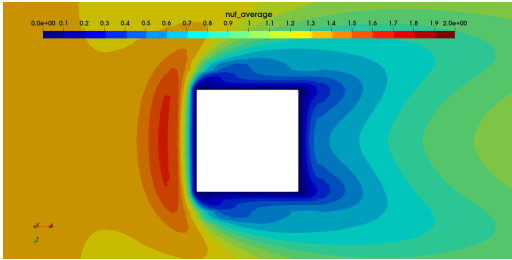


(d) Turbulent kinetic energy (k) field in the cross-sectional plane for the STD $k-\omega$ model at 0°

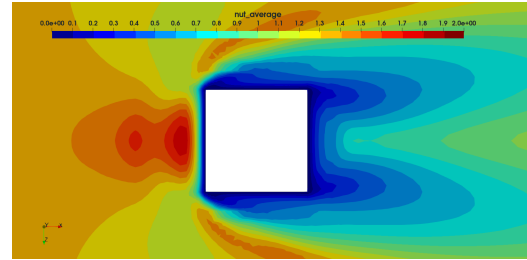


(e) Turbulent kinetic energy (k) field in the cross-sectional plane for the SST $k-\omega$ model at 0°

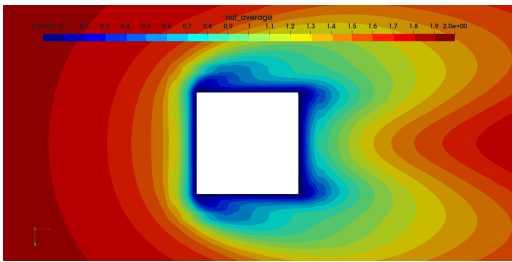
Figure 2.55: Cross-sectional turbulent kinetic energy (k) field for turbulence models at 0°



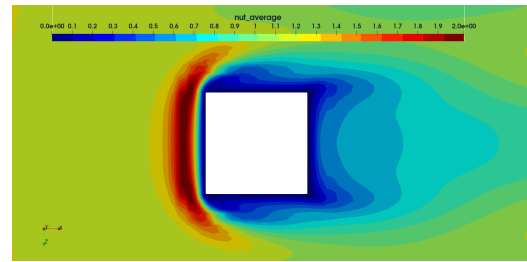
(a) Turbulent viscosity (ν_t) field in the cross-sectional plane for the STD $k-\epsilon$ model at 0°



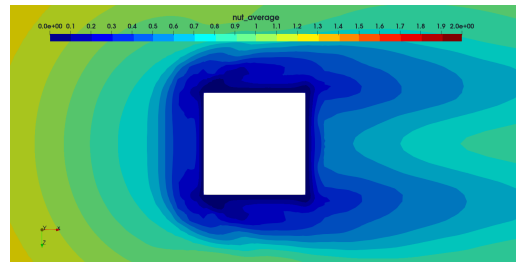
(b) Turbulent viscosity (ν_t) field in the cross-sectional plane for the Realizable $k-\epsilon$ model at 0°



(c) Turbulent viscosity (ν_t) field in the cross-sectional plane for the RNG $k-\epsilon$ model at 0°

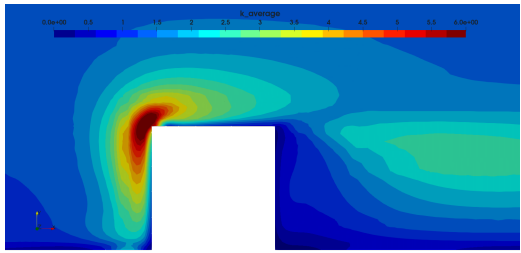


(d) Turbulent viscosity (ν_t) field in the cross-sectional plane for the STD $k-\omega$ model at 0°

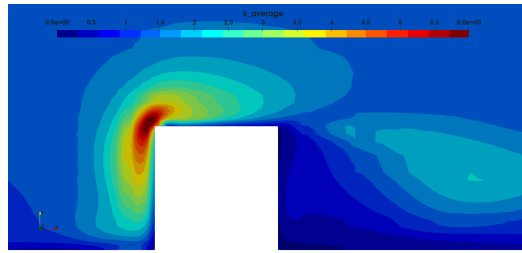


(e) Turbulent viscosity (ν_t) field in the cross-sectional plane for the SST $k-\omega$ model at 0°

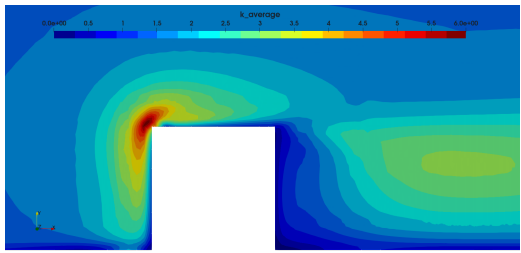
Figure 2.56: Cross-sectional turbulent viscosity (ν_t) field for turbulence models at 0°



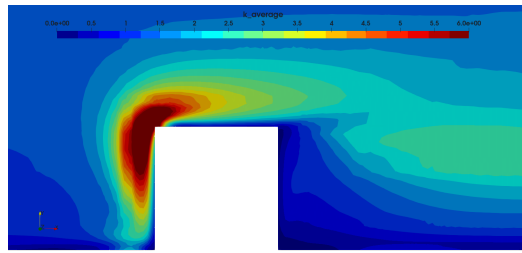
(a) Turbulent kinetic energy (k) field in the parallel flow plane for the STD k - ϵ model at 15°



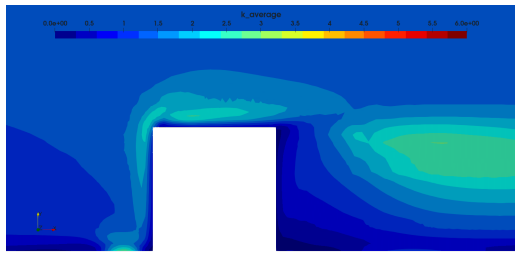
(b) Turbulent kinetic energy (k) field in the parallel flow plane for the Realizable k - ϵ model at 15°



(c) Turbulent kinetic energy (k) field in the parallel flow plane for the RNG k - ϵ model at 15°

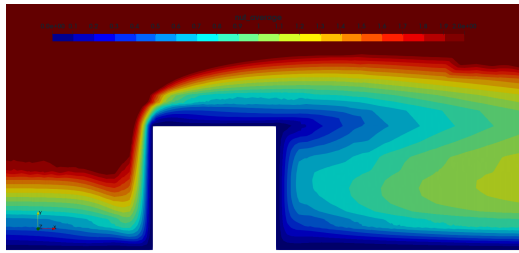


(d) Turbulent kinetic energy (k) field in the parallel flow plane for the STD k - ω model at 15°

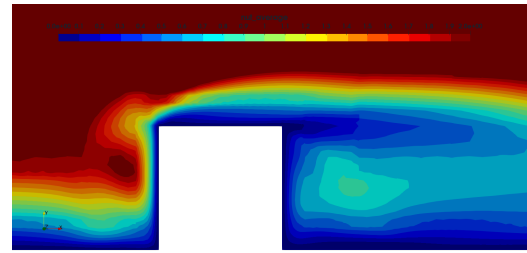


(e) Turbulent kinetic energy (k) field in the parallel flow plane for the SST k - ω model at 15°

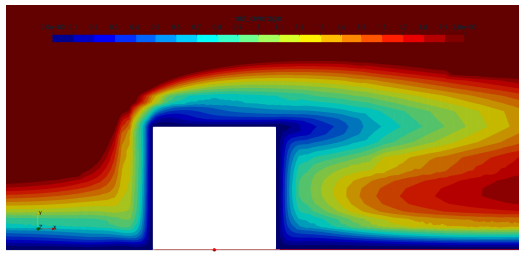
Figure 2.57: Turbulent kinetic energy (k) field in the parallel flow plane for turbulence models at 15°



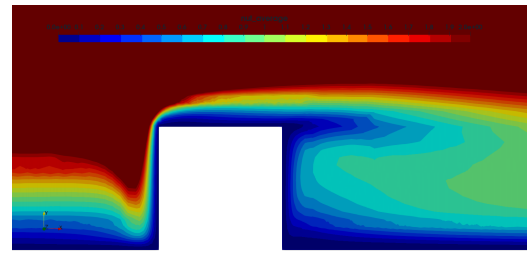
(a) Turbulent viscosity (ν_t) field in the parallel flow plane for the STD $k-\epsilon$ model at 15°



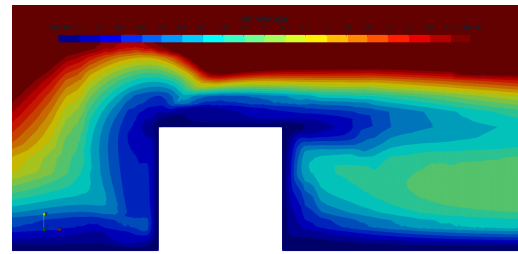
(b) Turbulent viscosity (ν_t) field in the parallel flow plane for the Realizable $k-\epsilon$ model at 15°



(c) Turbulent viscosity (ν_t) field in the parallel flow plane for the RNG $k-\epsilon$ model at 15°

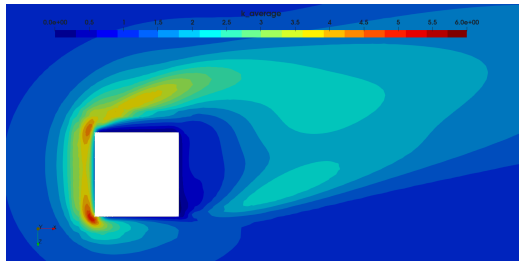


(d) Turbulent viscosity (ν_t) field in the parallel flow plane for the STD $k-\omega$ model at 15°

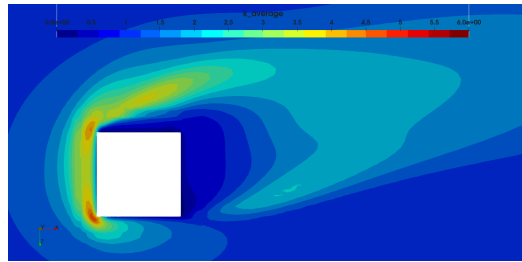


(e) Turbulent viscosity (ν_t) field in the parallel flow plane for the SST $k-\omega$ model at 15°

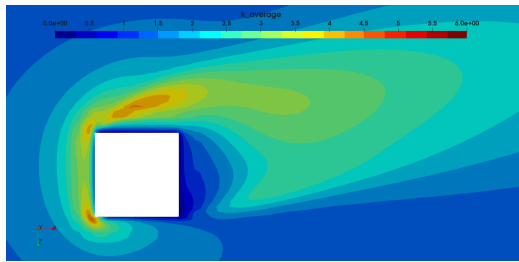
Figure 2.58: Turbulent viscosity (ν_t) field in the parallel flow plane for turbulence models at 15°



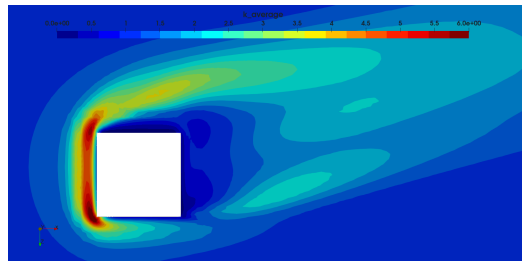
(a) Turbulent kinetic energy (k) field in the cross-sectional plane for the STD $k-\epsilon$ model at 15°



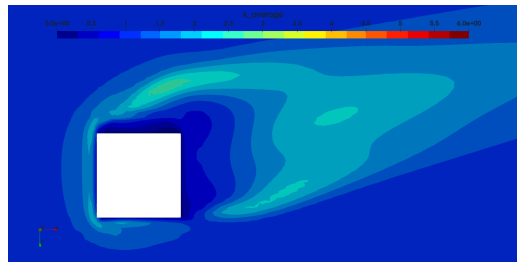
(b) Turbulent kinetic energy (k) field in the cross-sectional plane for the Realizable $k-\epsilon$ model at 15°



(c) Turbulent kinetic energy (k) field in the cross-sectional plane for the RNG $k-\epsilon$ model at 15°

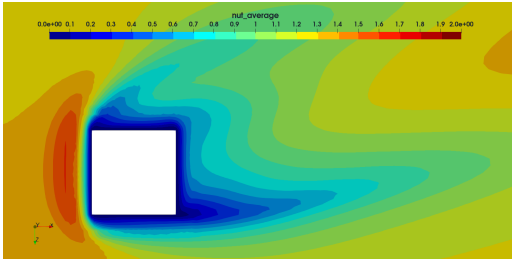


(d) Turbulent kinetic energy (k) field in the cross-sectional plane for the STD $k-\omega$ model at 15°

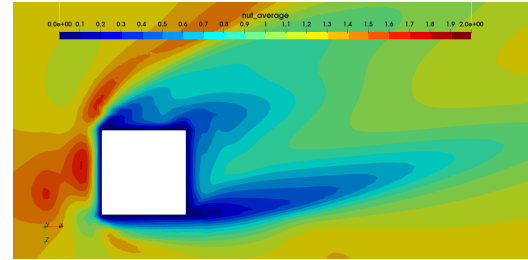


(e) Turbulent kinetic energy (k) field in the cross-sectional plane for the SST $k-\omega$ model at 15°

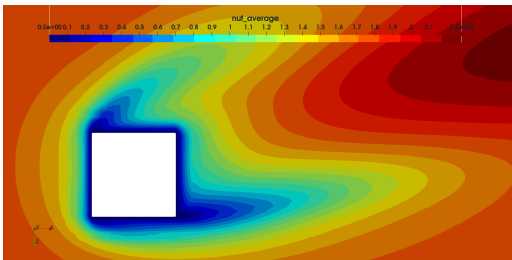
Figure 2.59: Cross-sectional turbulent kinetic energy (k) field for turbulence models at 15°



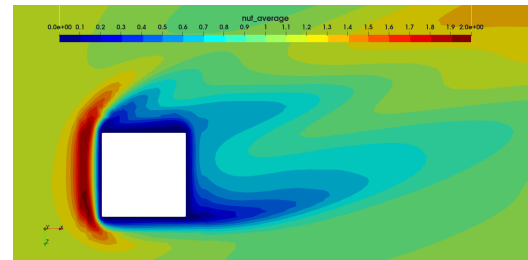
(a) Turbulent viscosity (ν_t) field in the cross-sectional plane for the STD $k-\epsilon$ model at 15°



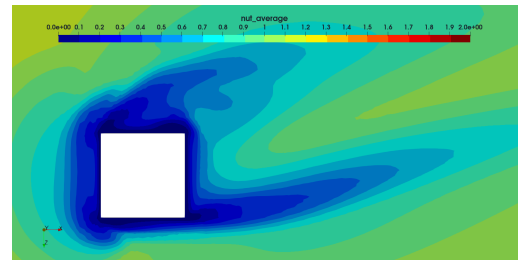
(b) Turbulent viscosity (ν_t) field in the cross-sectional plane for the Realizable $k-\epsilon$ model at 15°



(c) Turbulent viscosity (ν_t) field in the cross-sectional plane for the RNG $k-\epsilon$ model at 15°

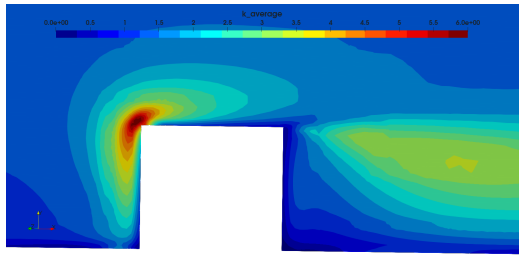


(d) Turbulent viscosity (ν_t) field in the cross-sectional plane for the STD $k-\omega$ model at 15°

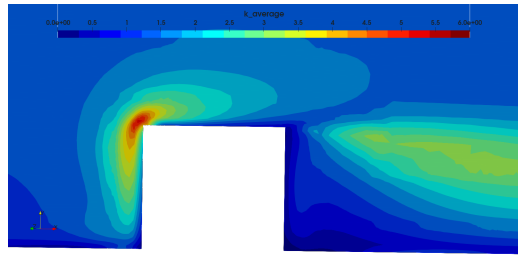


(e) Turbulent viscosity (ν_t) field in the cross-sectional plane for the SST $k-\omega$ model at 15°

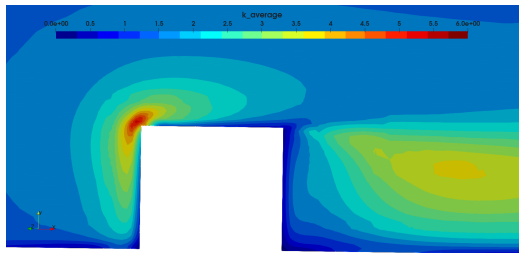
Figure 2.60: Cross-sectional turbulent viscosity (ν_t) field for turbulence models at 15°



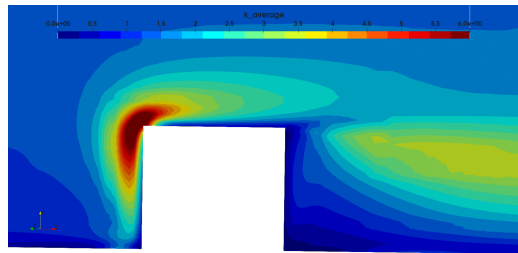
(a) Turbulent kinetic energy (k) field in the parallel flow plane for the STD k - ϵ model at 30°



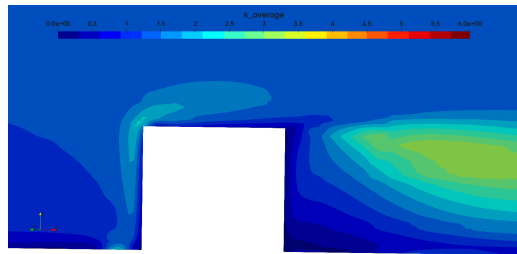
(b) Turbulent kinetic energy (k) field in the parallel flow plane for the Realizable k - ϵ model at 30°



(c) Turbulent kinetic energy (k) field in the parallel flow plane for the RNG k - ϵ model at 30°

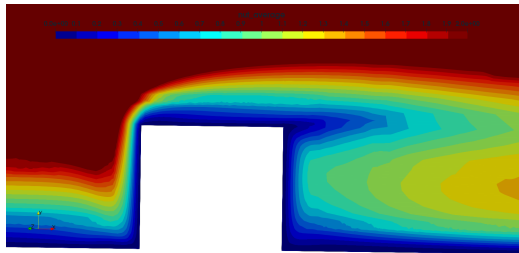


(d) Turbulent kinetic energy (k) field in the parallel flow plane for the STD k - ω model at 30°

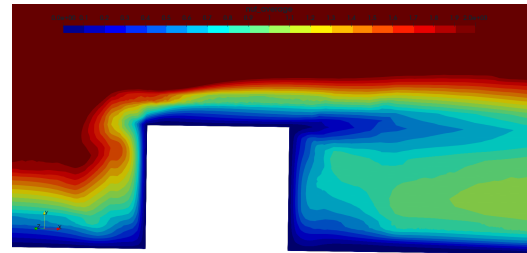


(e) Turbulent kinetic energy (k) field in the parallel flow plane for the SST k - ω model at 30°

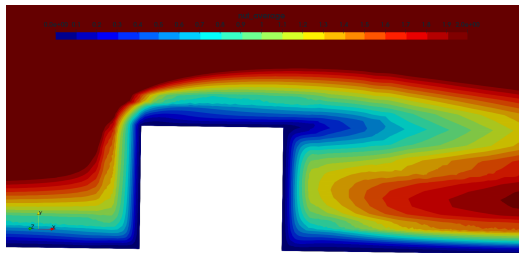
Figure 2.61: Turbulent kinetic energy (k) field in the parallel flow plane for turbulence models at 30°



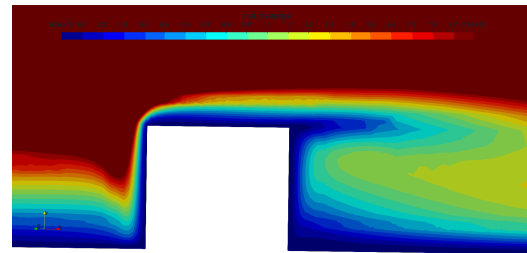
(a) Turbulent viscosity (ν_t) field in the parallel flow plane for the STD $k-\epsilon$ model at 30°



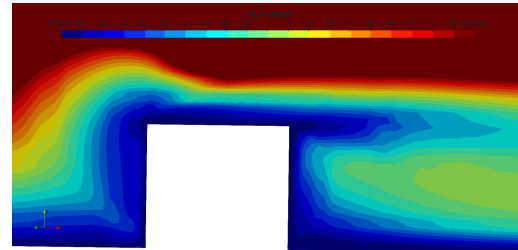
(b) Turbulent viscosity (ν_t) field in the parallel flow plane for the Realizable $k-\epsilon$ model at 30°



(c) Turbulent viscosity (ν_t) field in the parallel flow plane for the RNG $k-\epsilon$ model at 30°

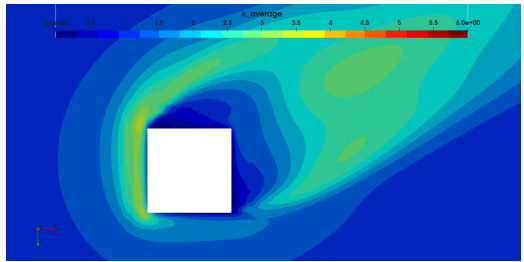


(d) Turbulent viscosity (ν_t) field in the parallel flow plane for the STD $k-\omega$ model at 30°

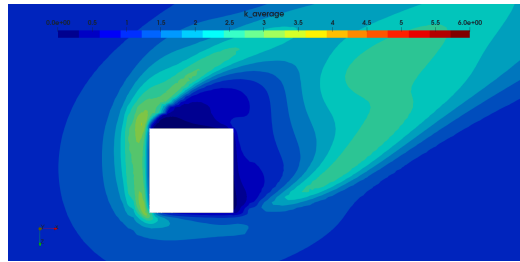


(e) Turbulent viscosity (ν_t) field in the parallel flow plane for the SST $k-\omega$ model at 30°

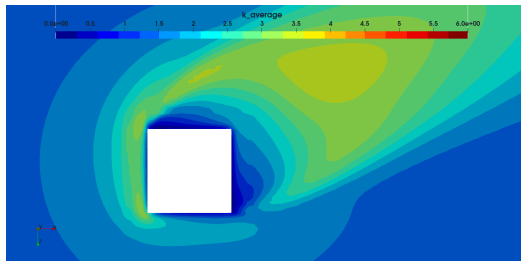
Figure 2.62: Turbulent viscosity (ν_t) field in the parallel flow plane for turbulence models at 30°



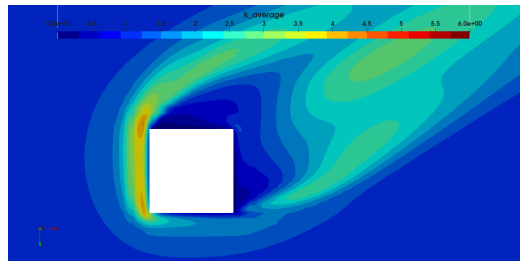
(a) Turbulent kinetic energy (k) field in the cross-sectional plane for the STD $k-\epsilon$ model at 30°



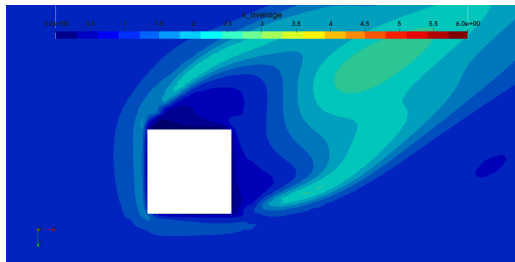
(b) Turbulent kinetic energy (k) field in the cross-sectional plane for the Realizable $k-\epsilon$ model at 30°



(c) Turbulent kinetic energy (k) field in the cross-sectional plane for the RNG $k-\epsilon$ model at 30°

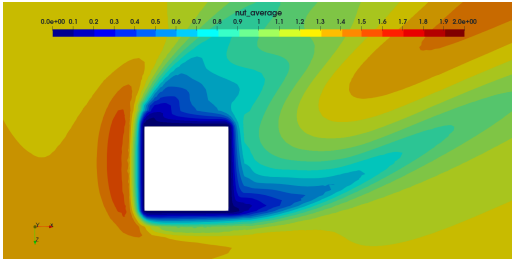


(d) Turbulent kinetic energy (k) field in the cross-sectional plane for the STD $k-\omega$ model at 30°

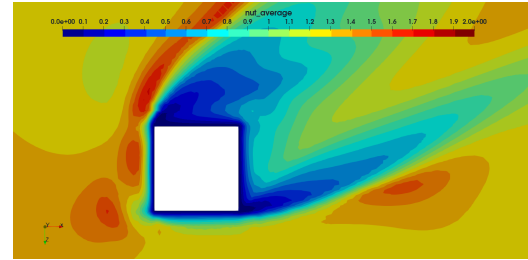


(e) Turbulent kinetic energy (k) field in the cross-sectional plane for the SST $k-\omega$ model at 30°

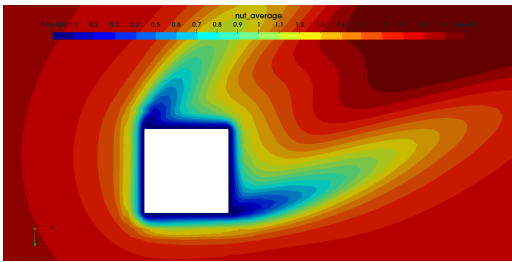
Figure 2.63: Cross-sectional turbulent kinetic energy (k) field for turbulence models at 30°



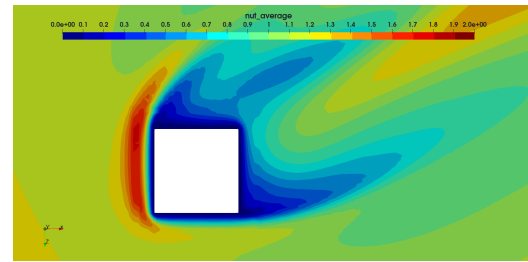
(a) Turbulent viscosity (ν_t) field in the cross-sectional plane for the STD $k-\epsilon$ model at 30°



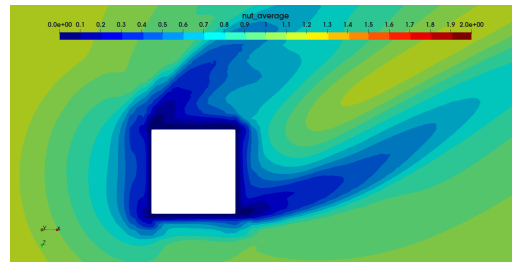
(b) Turbulent viscosity (ν_t) field in the cross-sectional plane for the Realizable $k-\epsilon$ model at 30°



(c) Turbulent viscosity (ν_t) field in the cross-sectional plane for the RNG $k-\epsilon$ model at 30°

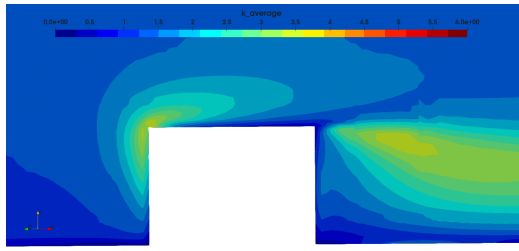


(d) Turbulent viscosity (ν_t) field in the cross-sectional plane for the STD $k-\omega$ model at 30°

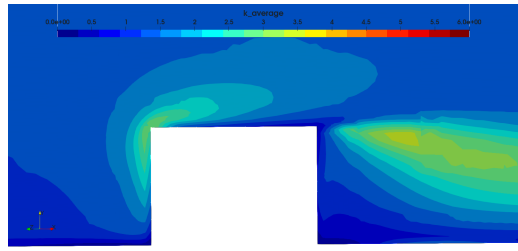


(e) Turbulent viscosity (ν_t) field in the cross-sectional plane for the SST $k-\omega$ model at 30°

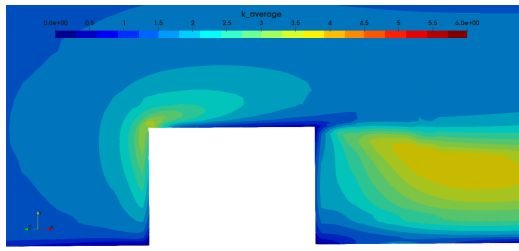
Figure 2.64: Cross-sectional turbulent viscosity (ν_t) field for turbulence models at 30°



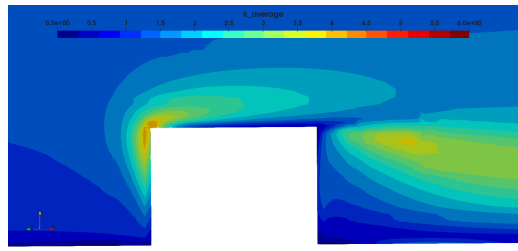
(a) Turbulent kinetic energy (k) field in the parallel flow plane for the STD k - ϵ model at 45°



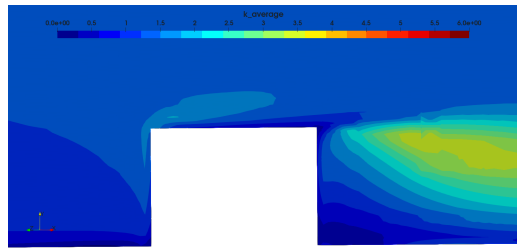
(b) Turbulent kinetic energy (k) field in the parallel flow plane for the Realizable k - ϵ model at 45°



(c) Turbulent kinetic energy (k) field in the parallel flow plane for the RNG k - ϵ model at 45°



(d) Turbulent kinetic energy (k) field in the parallel flow plane for the STD k - ω model at 45°



(e) Turbulent kinetic energy (k) field in the parallel flow plane for the SST k - ω model at 45°

Figure 2.65: Turbulent kinetic energy (k) field in the parallel flow plane for turbulence models at 45°

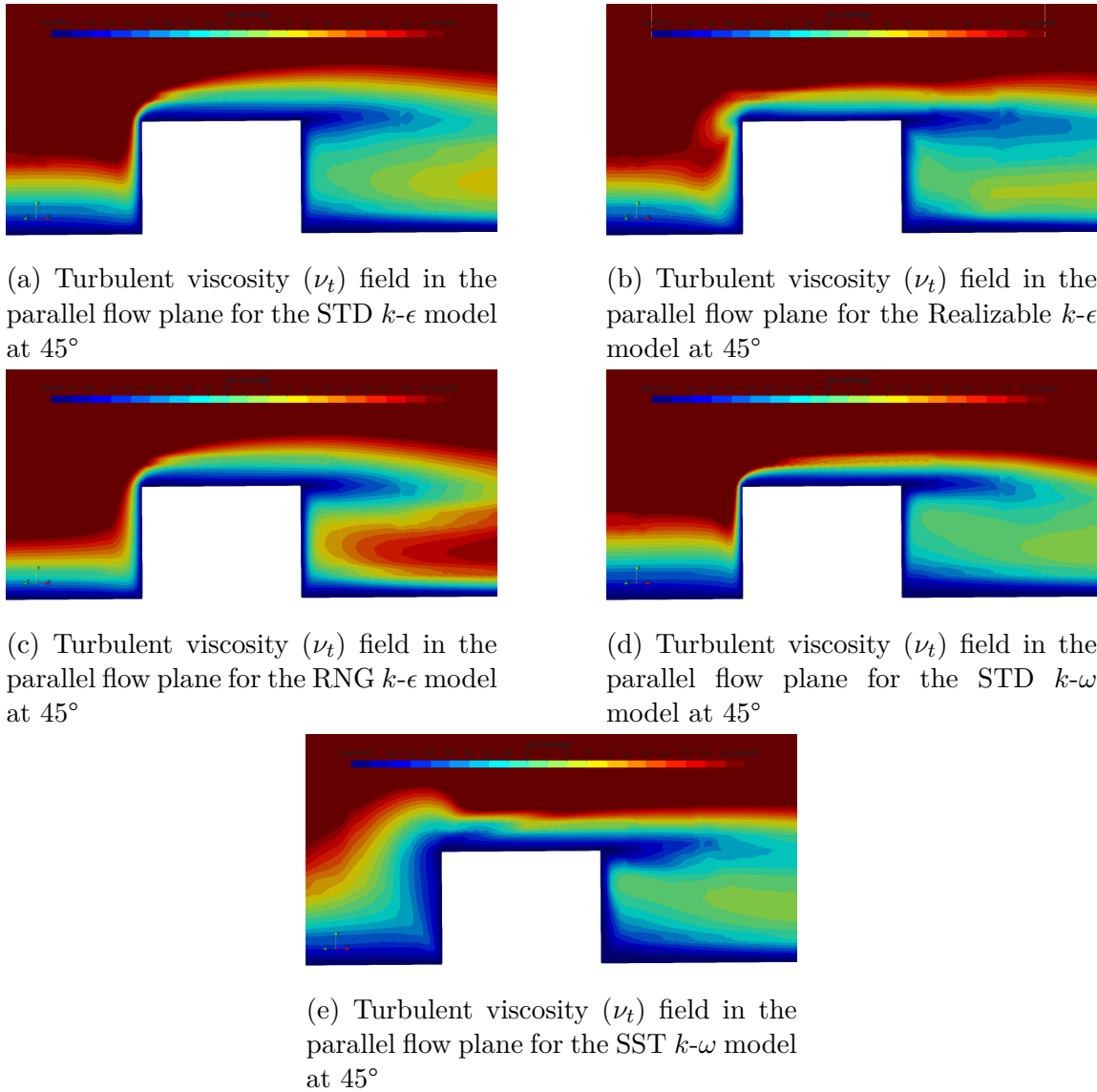
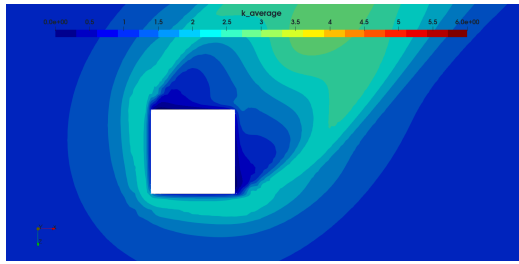
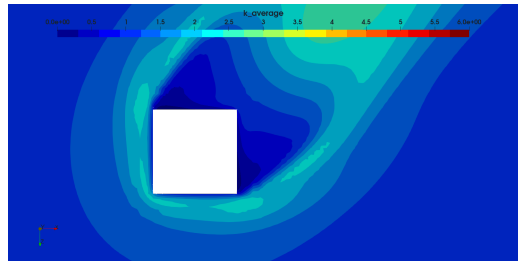


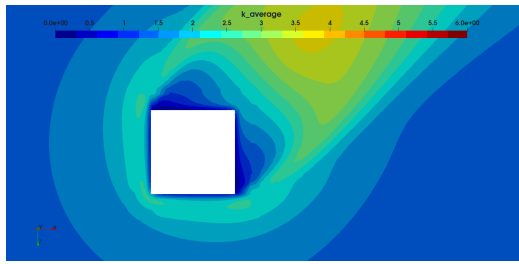
Figure 2.66: Turbulent viscosity (ν_t) field in the parallel flow plane for turbulence models at 45°



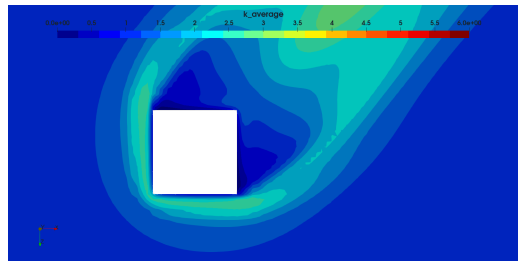
(a) Turbulent kinetic energy (k) field in the cross-sectional plane for the STD k - ϵ model at 45°



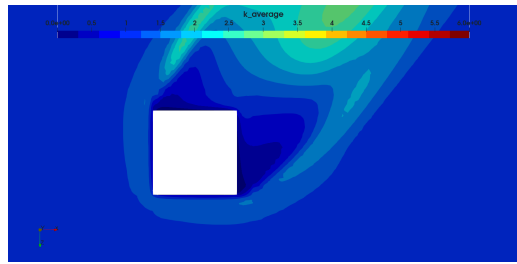
(b) Turbulent kinetic energy (k) field in the cross-sectional plane for the Realizable k - ϵ model at 45°



(c) Turbulent kinetic energy (k) field in the cross-sectional plane for the RNG k - ϵ model at 45°

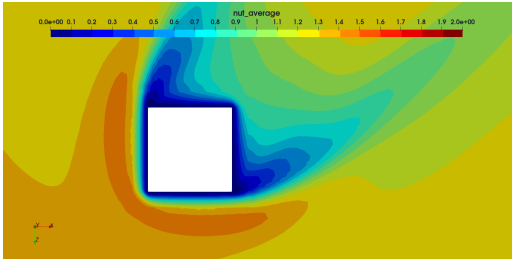


(d) Turbulent kinetic energy (k) field in the cross-sectional plane for the STD k - ω model at 45°

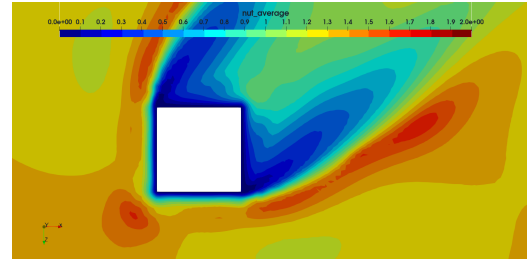


(e) Turbulent kinetic energy (k) field in the cross-sectional plane for the SST k - ω model at 45°

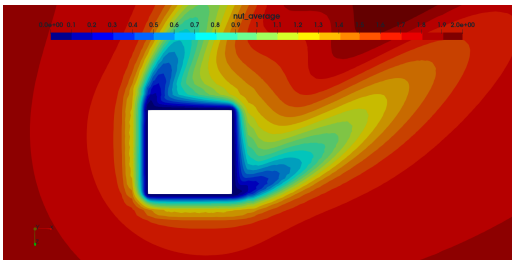
Figure 2.67: Cross-sectional turbulent kinetic energy (k) field for turbulence models at 45°



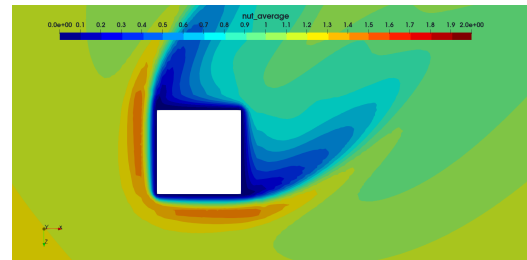
(a) Turbulent viscosity (ν_t) field in the cross-sectional plane for the STD $k-\epsilon$ model at 45°



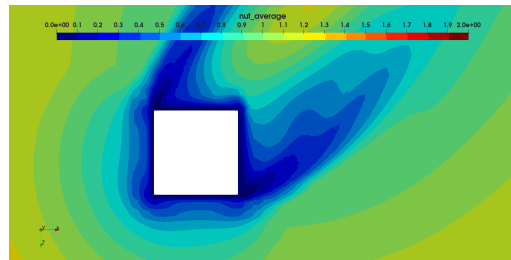
(b) Turbulent viscosity (ν_t) field in the cross-sectional plane for the Realizable $k-\epsilon$ model at 45°



(c) Turbulent viscosity (ν_t) field in the cross-sectional plane for the RNG $k-\epsilon$ model at 45°



(d) Turbulent viscosity (ν_t) field in the cross-sectional plane for the STD $k-\omega$ model at 45°



(e) Turbulent viscosity (ν_t) field in the cross-sectional plane for the SST $k-\omega$ model at 45°

Figure 2.68: Cross-sectional turbulent viscosity (ν_t) field for turbulence models at 45°

2.6 Stream-lines

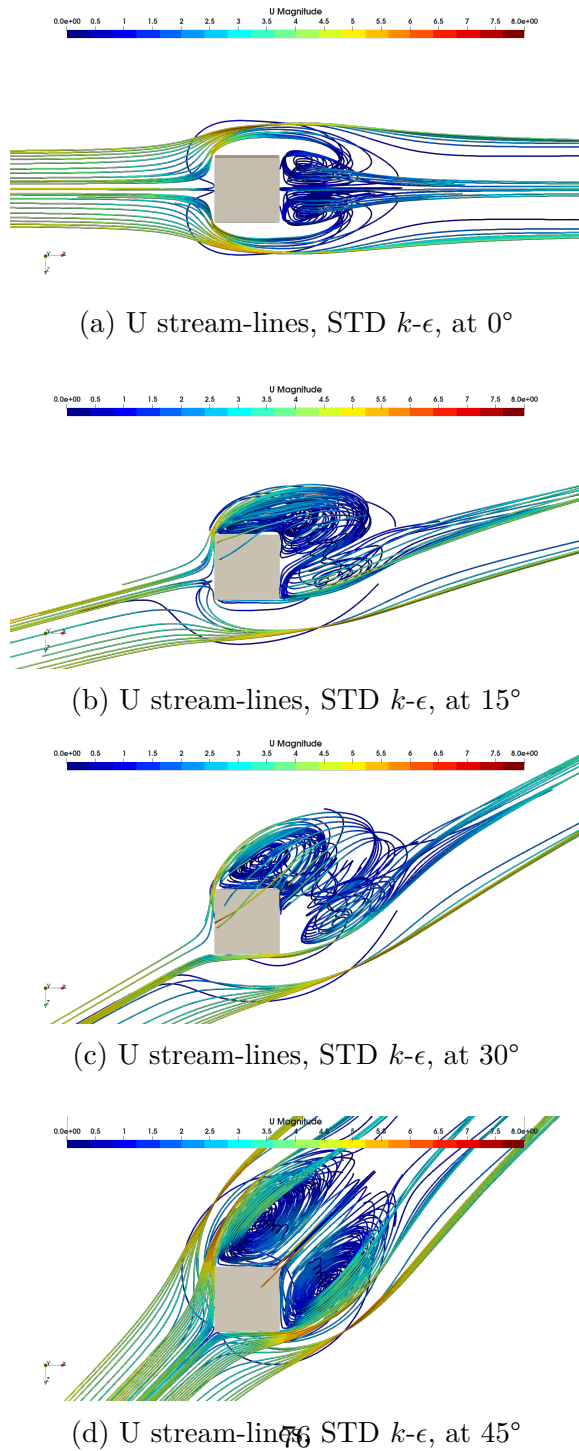
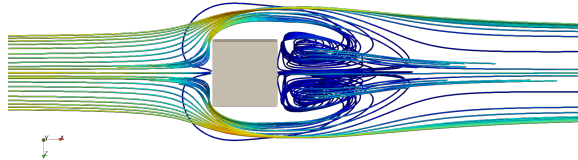
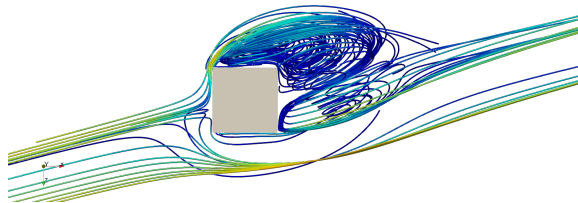
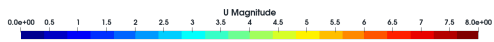


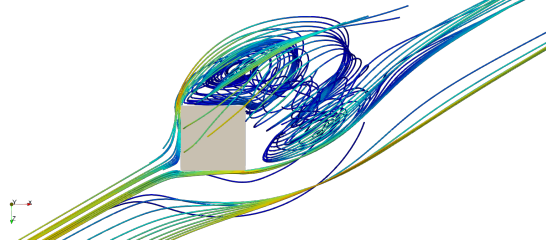
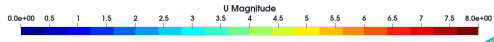
Figure 2.69: U stream-lines, STD $k-\epsilon$



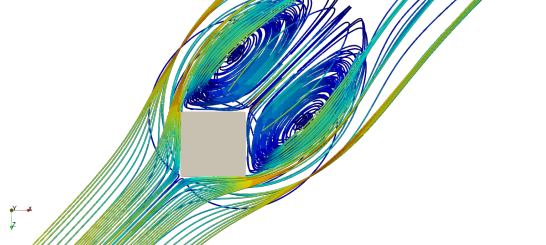
(a) U stream-lines, Realizable $k-\epsilon$, at 0°



(b) U stream-lines, Realizable $k-\epsilon$, at 15°

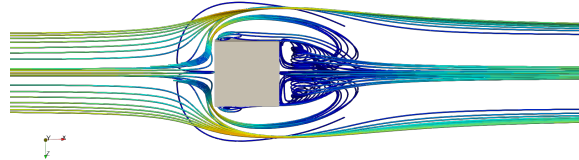
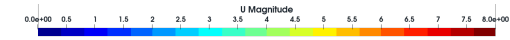


(c) U stream-lines, Realizable $k-\epsilon$, at 30°

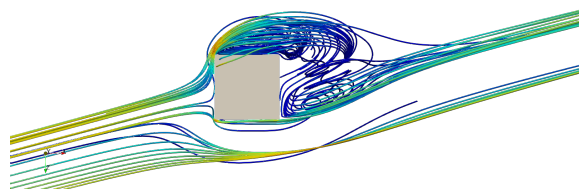
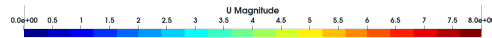


(d) U stream-lines, Realizable $k-\epsilon$, at 45°

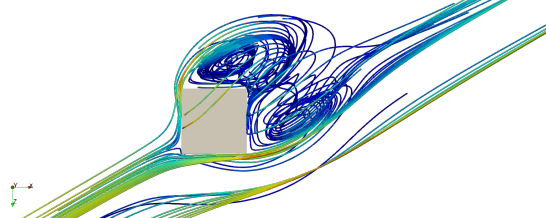
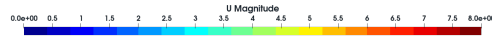
Figure 2.70: U stream-lines, Realizable $k-\epsilon$



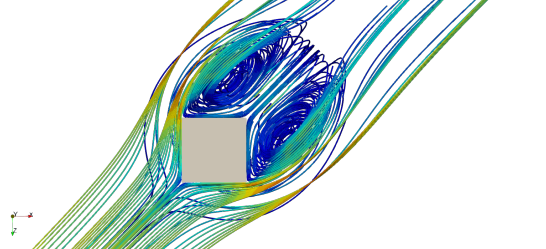
(a) U stream-lines, RNG $k-\epsilon$, at 0°



(b) U stream-lines, RNG $k-\epsilon$, at 15°

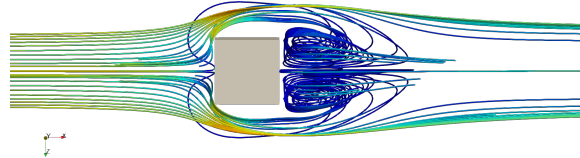
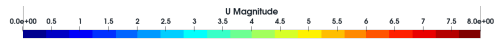


(c) U stream-lines, RNG $k-\epsilon$, at 30°

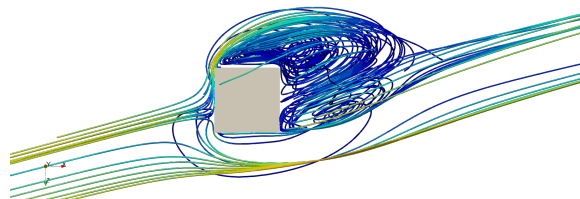
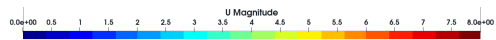


(d) U stream-lines, RNG $k-\epsilon$, at 45°

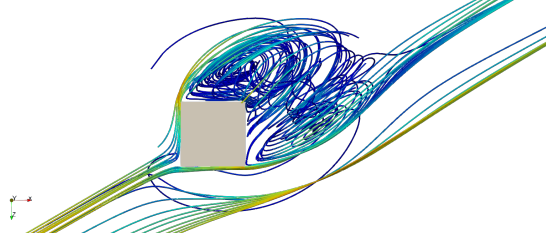
Figure 2.71: U stream-lines, RNG $k-\epsilon$



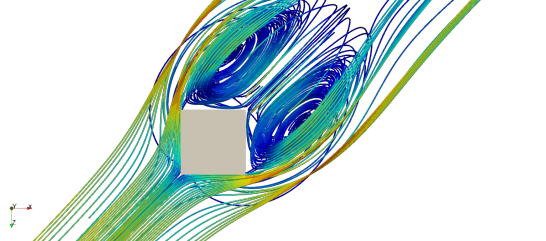
(a) U stream-lines, STD $k-\omega$, at 0°



(b) U stream-lines, STD $k-\omega$, at 15°

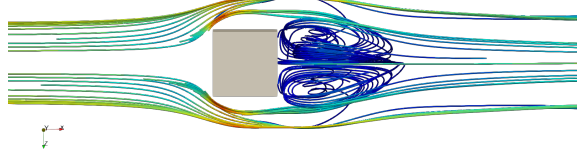
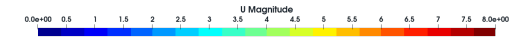


(c) U stream-lines, STD $k-\omega$, at 30°

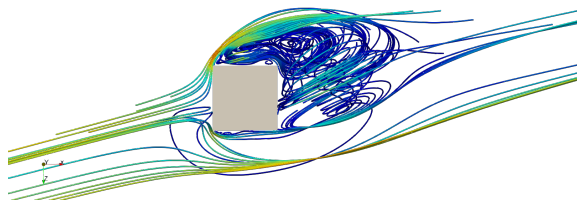
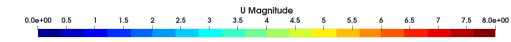


(d) U stream-lines, STD $k-\omega$, at 45°

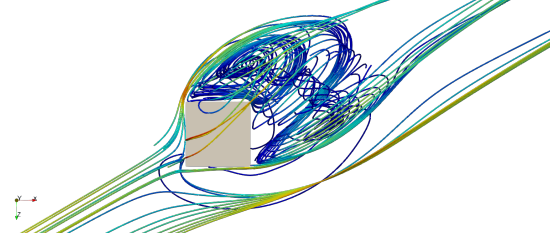
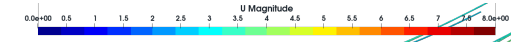
Figure 2.72: U stream-lines, STD $k-\omega$



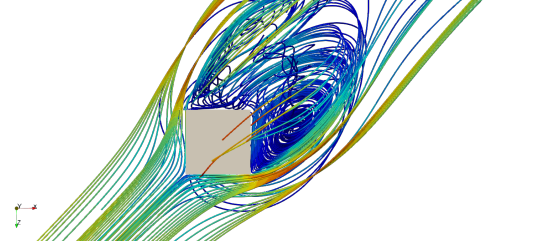
(a) U stream-lines, SST $k-\omega$, at 0°



(b) U stream-lines, SST $k-\omega$, at 15°



(c) U stream-lines, SST $k-\omega$, at 30°



(d) U stream-lines, SST $k-\omega$, at 45°

Figure 2.73: U stream-lines, SST $k-\omega$